

CHAPTER 1

INTRODUCTION

1.1 Introduction

Gas Metal Arc Welding is a process in which the source of heat is an arc format between consumable metal electrode and the work piece, and the arc and the molten puddle are protected from contamination by the atmosphere (i.e. oxygen and nitrogen) with an externally supplied gaseous shield of gas either inert such as argon, helium or an argon-helium mixture or active such as carbon dioxide, argon-carbon dioxide mixture, which is chemically active or not inert [1]. Initially GMAW was called as MIG Welding because only inert gasses were used to protect the molten puddle. The application of this process was restricted to aluminum, deoxidized copper and silicon bronze. Later it was used to weld ferrite and austenitic steels, and mild steel successfully by using active gasses in place of inert gasses and hence was term MAG (Metal Active Gas) welding [2]. All the major commercial metals can be welded by GMAW (MIG/CO₂) process, including carbon steels, low alloy and high alloy steels, stainless, aluminum, and copper titanium, zirconium and nickel alloys. [3]. GMAW welding process overcome the restriction of using small lengths of electrodes and overcome the inability of the submerged-arc process to weld in various positions. By

suitable adjusting the process parameters, it is possible to weld joints in the thickness range of 1-13 mm in all welding position.

Several researchers have attempted to investigate the effects of various process variables on the weld bead geometry and metal transfer. The quality of any weld process is characterized by the weld distortion, mechanical properties and weld bead geometry. Out of these factors, the weld bead geometry is the easiest to measure and control. Thus by controlling the weld bead geometry we can successfully control the weld quality. But the relationship between the process variables and the weld bead geometry is very complex and necessitates a robust mathematical approach to quantify the relationship between them.

Synergic MIG is an advanced welding system which incorporates both spray and pulse transfer. It is a complete range of high technology digital microprocessor controlled equipment. Optimum conditions can be established for a range of applications which are readily reproduced by the welder. **Synergic** means “to work together” and in connection with the welding process it indicates that the welding machine is capable of choosing the current curve when the welder has set the wire speed, the metal alloy, the wire diameter and the shielding gas. That is the welding equipment controls the base current, the form and number of the current pulsations. The synergic capability enabled all of the welding parameters to be controlled from a signal dial control which optimized the current peak pulse and background values, the voltage, wire feed speed. It has also become possible to reprogram the power source instantly when wire size, shield gas, filler metal composition, etc. are changed, simply

by dialing in a programmer number. These programmes have been established by the equipment manufacturer with the optimum parameters for the application.

Apart from influencing the bead geometry, the input process variables also affect the metallurgical aspects of the metal being joined. The micro hardness, the different phases constituting the micro structure, the percentage of different phases, grain size etc. are largely influenced by the input process variables and ultimately they affect the performance of the welded metal in different applications.

1.2 Motivation and Objectives

The motivation of this project was provided by desire to explore the frontiers of welding technology, which form the backbone of manufacturing industries. To be able to successfully use a process in industry it is imperative that we have a robust way of controlling the outputs as per our needs.

The main objective of this project was to understand the influence of process variables such as Arc Voltage, Current, plate thickness, gas flow rate, wire feed rate and Travel Speed on the bead geometry features and to quantify the relationships through development of mathematical models. The effect of welding parameters on metallurgy was also studied.

1.3 Statement of the Problem

“Experimental investigation and statistical analysis of various parameters in synergic MIG welding of 304L stainless steel”

The research work describes the optimization of experimental observations made on stainless steel plate through bead-on-plate technique using RSM and the metallurgical aspects of the welded metal were also studied and an attempt was made to co-relate the observed values with the input process variables.

1.4 Plan of Investigation

The research work was planned to be carried out in following steps:

1. Identification of important process control variables
2. Deciding the working range of the process control variables, viz. Welding Current(A), plate thickness(T), gas flow rate(G), and Travel Speed (S)
3. Developing the design matrix
4. Conducting the experiments as per the design matrix
5. Recording the responses viz. bead height (H), bead width (W) and bead penetration (P)
6. Developing the mathematical models
7. Checking the adequacy of the models
8. Finding the significance of co-efficient
9. Developing the final proposed models
10. Plotting of graphs and drawing conclusions
11. Finding the micro hardness and micro structure
12. Metallurgical analysis to co-relate the micro hardness and the micro structure of the welded material with the process variables
13. Discussion of the results

CHAPTER 2

LITERATURE REVIEW

2.1 Introduction

Welding is a fabrication process that joins two metals or non-metals by producing coalescence between them. This is generally achieved by heating the specimen up to their melting temperature with or without the addition of filler materials, to form a pool of molten metal that cool and solidifies to become a strong joint. While often an industrial process, welding can be done in many different environments, including open air, under water and in outer space. The studies of the effects of various welding process parameters on the formation of bead and bead geometry have attracted the attention of many researchers to carry out further investigations. Design of experiment (DOE) combined with Response surface methodology (RSM) is a powerful statistical tool to determine and represent the cause and effect relationship between responses and input control variables influencing the responses as a two or three dimensional hyper surface.

Many researchers and academicians of international repute have probed into the topic of study of effect of welding parameters on weld geometry and the mechanical performance and application of any welded joint is affected by the metallurgical properties of the welded joints. The present literature review has been carried out in the areas concerning the influence of input process variables in the bead geometry, application of RSM to develop mathematical models to model the relationships between

the inputs and the outputs of a process, and prediction of outputs and influence of process variables on the metallurgical changes taking place during welding.

- **Kim I.S., Basu A and siores E.**[4] studied the effect of welding process parameters on weld bead penetration Gas Metal Arc Welding (GMAW) process. Welding process parameters included wire diameter, gas flow rate, welding speed, arc current and arc voltage. The experiment results revealed that weld bead penetration increased as wire diameter, arc current and voltage increased.
- **Kim I.S, Son K.J., Yang and Yaragada** [5] developed a mathematical model for selection of process parameters and prediction of bead geometry in robotic GMAW. They used factorial design as a guide for optimization of process parameters. Three factors were incorporated into the model: arc current welding voltage and welding speed. The study revealed that a change of process parameters effects the bead width and height more strongly than penetration relatively.
- **Ganjigatti J.P., Pratihari D.K, and Roychoudhury A.**[6] studied an input output relationship of MIG Welding process by using regression analysis based on the data collected as per full factorial design of experiments. The effect of welding parameters and their interaction terms on different responses analyzed using statistical methods. Both linear as well as nonlinear regression analyses were employed to establish the input –output relations.

- **Ganjigatti J.P., Pratihari D.K, and Roychoudhury A.[7]** studied global versus cluster-wise regression analyses for prediction of bead geometry in MIG Welding process . They observed that the cluster-wise regression analyses performs slightly better than the global approach in predicting weld bead geometric parameters.

- **Erdal Karadeniz et al [8]** in their study, the effects of various welding parameters on welding penetration in Erdemir 6842 steel having 2.5 mm thickness welded by robotic gas metal arc welding were investigated. The welding current, arc voltage and welding speed were chosen as variable parameters. The depths of penetration were measured for each specimen after the welding operations and the effects of these parameters on penetration were researched. The study revealed that increasing welding current increased the depth of penetration. In addition, arc voltage is another parameter in incrimination of penetration.

- **Pires RM, Quintino I, Miranda L.[9]** describes the influences of the gases on the stability of the joining process and of the melted metal transfer through the electric arc. The influence of the type of the gas and welding speed, as well as other process parameters are addressed. The bead appearance and shape are analyzed, mainly underscoring the gases influences on the convexity of the bead, its colour, brightness, smoothness and surface pores formation.

- **P.K. Palani, N. Murugan [10]** developed a mathematical model for prediction of weld bead geometry in cladding by flux cored arc welding. The experiments were

conducted by depositing Type AISI 317L flux cored stainless steel wire onto IS: 2062 structural steel base plate. The results of the confirmation experiments showed that the models developed are able to predict the bead geometries and dilution with reasonable accuracy. The studies have indicated that both main and interaction effects of the process variables play a major role in determining the bead dimensions and dilution, and the effect of interaction between the process variables cannot be neglected. The process parameters were also optimized using response surface methodology (RSM) which will help the plant engineers to select and control the process variables effectively, to achieve the desired clad qualities.

- **Manoj Singla, Dharminder Singh, Dharmpal Deepak [11]** studied optimizing various Gas Metal Arc welding parameters including welding voltage, welding current, welding speed and nozzle to plate distance (NPD) by developing a mathematical model for sound weld deposit area of a mild steel specimen. Factorial design approach has been applied for finding the relationship between the various process parameters and weld deposit area. The study revealed that the welding voltage and NPD varies directly with weld deposit area and inverse relationship is found between welding current and speed with weld deposit area.
- **Gunaraj and Murugan [12]** have highlighted the use of RSM to develop mathematical models and plot contour graphs relating important input parameters namely the open-circuit voltage, wire feed-rate, welding speed and nozzle- to-plate distance to some responses namely, the penetration,

reinforcement, width and percentage dilution of the weld bead in SAW of pipes. They demonstrated that all responses decrease with increasing welding speed. Also, when the nozzle-to-plate distance increases all responses decrease, but reinforcement increases. Moreover, an increase in the wire feed-rate results in an increase in all responses but the width remains unchanged.

- **Gunaraj and Murugan [13]** studied the effect of SAW parameters on the heat input and the area of HAZ for low-carbon steel with two joint types, bead-on-plate and bead-on-joint, using mathematical models developed by RSM. They found that for the same heat input, the area of the HAZ is greater for the bead-on-plate than that for bead-on-joint. They found that the effect of SAW parameters on the area of HAZ in both cases follows the same trend.
- **Murugan N. and Parmar R.S and Sud S.K.[14]** used response surface methodology to established quadratic relations between welding parameters and bead geometry for depositing stainless steel into structure steel, using automated Submerged arc welding.
- **Murugan N. and Parmar R.S [15]** used response surface methodology to established quadratic relations between welding parameters and bead geometry for depositing stainless steel into structure steel, using gas metal arc welding process
- **Shahi A.S. and Pandey Sunil [16]** studied the effects of welding conditions on dilution of stainless steel cladding produced by gas metal arc welding.

Experimental study carried out to analyze the effect of various gas metal arc welding (GMAW) and Universal gas metal arc welding (UGMAW) process parameters on dilution in single layer stainless steel cladding of low carbon structural steel plates. This comparative study revealed that dilution obtained in UGMAW process is significantly lower than that with GMAW process due to external preheating of the filler wire in UGMAW process which results in greater contribution of arc energy by resistive heating and as a consequence, significant drop in main welding current values in case of UGMAW process was observed.

- **Murugan and Gunaraj [17]** used 5 level 4 factor central composite rotatable design matrix for Prediction and control of weld bead geometry and shape relationships in submerged arc welding of pipes. Arc voltage, wire feed rate; welding speed and nozzle-to-plate distance were considered as the main factors affecting the bead geometry. Mathematical models have been developed for SAW of pipes using five level factorial techniques to predict three critical dimensions of the weld bead geometry and shape relationships. The models developed have been checked for their adequacy and significance by using the *F*-test and the *t*-test, respectively. Out of the four process variables considered, wire feed rate had a significant positive effect but welding speed had an appreciable negative effect on most of the important bead parameters. Penetration increased by about 1.3mm as wire feed rate was increased from -2 to +2 limits whereas penetration decreased by about 1mm as welding speed was increased from -2 to +2 limits. Arc voltage had a less significant negative effect on penetration and reinforcement but had a positive effect on bead width,

penetration size factor and reinforcement form factor. As wire feed rate had a positive effect but welding speed had a negative effect on most of the bead parameters, the interaction effects of wire feed and travel speed were similar for most of the parameters. Penetration, width, penetration size factor and reinforcement form factor all increased with the increase in wire feed rate for all values of welding speed but this increasing rate of the bead parameters with the increase in wire feed rate is gradually decreased with the increase in travel speed.

- **Koleva [18]** has carried out another work by applying RSM to establish the relationship between performance characteristics (weld-depth, weld-width and thermal efficiency) and its influencing factors (beam power, welding velocity, focus position, focusing current of the beam and the distance to the sample surface) for EBW of austenitic stainless steel. Optimal welding regimes were found through the thermal efficiency optimization. New statistical approaches were proposed to choose the focus position at a condition of maximum thermal efficiency and welding depth.
- **M. Eroglu et al [19]** carried out investigations to study the effect of coarse initial grain size on microstructure and mechanical properties of weld metal and HAZ of low carbon steel. In this study, the effects of coarse initial grain size with varying heat inputs on microstructure and mechanical properties of weld metal and heat-affected zone (HAZ) were investigated. Microstructure, hardness and toughness of weld metals and HAZs were investigated. From the results, they tried to

establish a relationship between initial grain size, microstructure, hardness and toughness of weld metals and HAZs. Considering the heat input, it was observed that the coarse initial grain size had a great influence on the microstructure, hardness and toughness of HAZ of low carbon steel. Thus, taking into consideration the plate thickness, a higher heat input should be used with respect to the maximum toughness of the HAZ in the welding of grain-coarsened low carbon steels.

- **D.V.Kiran Basu B and De A [20]** investigated the influence of process variables on weld bead quality in 2 wire tandem submerged arc welding of HSLA steel. In particular, the quantitative effects of the trailing wire current pulses and negative current pulse duration, leading wire current, and welding speed on the weld bead dimensions and mechanical properties are studied at fifty different sets of welding conditions that are designed following the principle of two-level, five factor central composite rotatable design. The experimental results show that the final weld bead width and reinforcement height are primarily influenced by the trailing wire current while the penetration is influenced by the leading wire current with the other conditions remaining constant. Increase in welding speed tends to reduce weld pool size leading to higher cooling rate that encourages greater volume fraction of acicular ferrite phase and better weld bead mechanical properties. The predictions of weld dimensions and mechanical properties from the empirical relations, which are developed based on the experimental results, are in fair agreement with the corresponding measured values within the ranges of the welding conditions considered in the work.

- **Gunaraj et al [21]** developed mathematical models for prediction and comparison of area of the heat-affected zone for the bead-on-plate and bead-on-joint of pipes. The amount of heat input to the weld metal increases as voltage or wire feed rate or both increase. The heat input decreases with increase in travel speed. They found that voltage and wire feed rate had a positive effect on area of HAZ while travel speed and nozzle-to-plate distance had a negative effect. For the same heat input the area of HAZ is greater on the plate than on the joint. The direct and indirect effects of process variables on the area of the HAZ on both the bead-on-plate and the bead-on-joint are found to be the same. It is also found that the slopes of the individual plots are generally equal.
- **Kolhe et al [22]** carried out a detailed work in prediction of microstructure and mechanical properties of multi pass SAW. A detailed study on the microstructure, phase analysis and mechanical properties, HAZ width of SA weld metal multipass joint and heat-affected zone of 16mm thick mild steel plate was carried out. The various sub-zones in the microstructure were observed in the HAZ of SA weld are spheroidized, partially transformed, grain refined and grain coarsened. Welding heat input can control the percentage of phases in the welded structures. More variations in bulk hardness of the fractured samples were observed than welded samples. More HAZ width at top region of welded specimen was seen than that of bottom region. For increase in heat input the percentage of graphitic phase was slightly decreased whereas the percentage of ferrite sharply increased and finally the ferritic structures were observed. The

proportionate value of micro hardness was observed for low heat input whereas for increased heat input variations in hardness value was observed.

On the basis of literature review it is observed that independent work has been done in development of mathematical models for welding process, their modeling and metallurgical studies have been carried out independently. But an integrated approach of studying the effects of various welding process variables on bead geometric descriptors using 5 level full factorial central composite design, use of regression analysis to develop mathematical models for predicting the weld bead geometry and studying the influence of process parameters on the metallurgy of the welded specimen in MIG welding of plates is hardly found in any literature. The present research work attempts to address this issue.

CHAPTER 3

THEORY AND EXPERIMENTATION

3.1 MIG Welding

3.1.1 Introduction

Gas Metal Arc Welding is a process in which the source of heat is an arc format between consumable metal electrode and the work piece, and the arc and the molten puddle are protected from contamination by the atmosphere. The American Welding Society refers to the process Gas Metal Arc Welding process to cover inert as well as active shield gasses. GMAW is basically a semi-automatic process, in which the arc lengths of electrode and the feeding of the wire are automatically controlled.

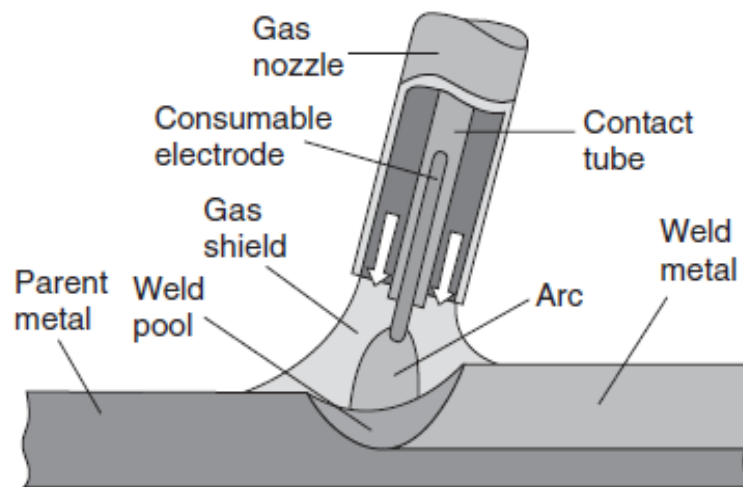


Fig3.1 Fundamental features of the MIG process. Courtesy of TWI Ltd.

The welding operator's job is reduced to positioning the gun at a correct angle and moving it along the seam at a controlled travel speed. Hence less operator skill is required with this process as compare to TIG and manual metal arc process. Yet basic training is required in the setting up of the equipment and manipulation of the gun must be provided to the operator to ensure quality GMAW welding [23, 24].

GMAW welding process overcome the restriction of using small lengths of electrodes and overcome the inability of the submerged-arc process to weld in various positions. By suitable adjusting the process parameters, it is possible to weld joints in the thickness range of 1-13 mm in all welding position [25]. All the major commercial metals can be welded by GMAW (MIG/CO₂) process, including carbon steels, low alloy and high alloy steels, stainless, aluminum, and copper titanium, zirconium and nickel alloys.



Fig3.2 Illustrating the general arrangement of the power source, wire feeder gas cylinder and work area, Courtesy of TWI Ltd.

The MIG welding process, illustrated in figs.3.1 and fig.3.2. As a rule uses direct current with the electrode connected to the positive pole of the power source, DC positive, or reverse polarity in the USA. Recent power source developments have been successful in enabling the MIG process to be also used with AC. Most of the heat developed in the arc is generated at the positive pole, in the case of MIG welding the electrode, resulting in high wire burn-off rates and an efficient transfer of this heat into the weld pool by means of the filler wire.

3.1.2 SYNERGIC MIG WELDING

Synergic MIG/MAG is an advanced welding system which incorporates both spray and pulse transfer. Optimum conditions can be established for a range of applications which are readily reproduced by the welder. **Synergic** means “to work together” and in connection with the welding process it indicates that the welding machine is capable of choosing the with current curve when the welder has set the wire speed, the metal alloy, the wire diameter and the shielding gas. That is the welding equipment controls the base current, the form and number of the current pulsations.

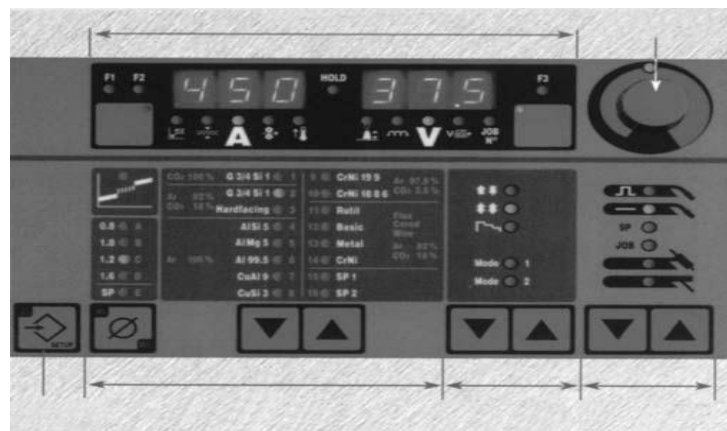


Fig.3.3 Typical modern pre-programmable control panel for synergic MIG power source. [2]

The synergic capability enabled all of the welding parameters to be controlled from a signal dial control which optimized the current peak pulse and background values, the voltage, wire feed speed. It has also become possible to reprogramme the power source instantly when wire size, shield gas, filler metal composition, etc. are changed, simply by dialing in a programme number (Fig.3.3). These programmes have been established by the equipment manufacturer with the optimum parameters for the application. Initially these units were expensive but the price has been steadily reduced such that they are now only marginally more costly than a conventional power source, leading to a far wider usage.

3.1.3 MECHANISM OF METAL TRANSFER

The **short-circuiting** or **dip transfer** mode, in which the metal melts to form large droplets whose diameter is often greater than that of the electrode wire. As the droplet forms at the end of the electrode, it makes contact with the weld pool and creates a short circuit, with a sudden increase in current. The surface tension causes a pinching effect which separates the droplet from the electrode. The frequency of this phenomenon is of the order of 20 to 100 Hz, corresponding to cycle times between 0.01 and 0.05 seconds.

The **globular transfer** or **gravity transfer** mode, as in the previous case, melting occurs in the form of large droplets, which break away when their mass is

sufficient to overcome surface tension forces and due to the greater arc length, fall freely before coming into contact with the weld pool.

The **spray transfer** mode involves current densities above a certain transition level, of the order of 200 A/mm^2 . The electrode melts to give a stream of fine droplets. As the current density increases further, the electrode tip becomes conical and the stream of even finer droplets is released axially.

In the GMAW (MIG) process, the metal transfer from the electrode tip to the weld pool across the arc is either globular, spray type or short-circuiting type depending upon many factors, which are enlisted as follows:

- The magnitude of welding current
- Shielding gas
- Current density
- Electrode extension and
- Electrode chemistry

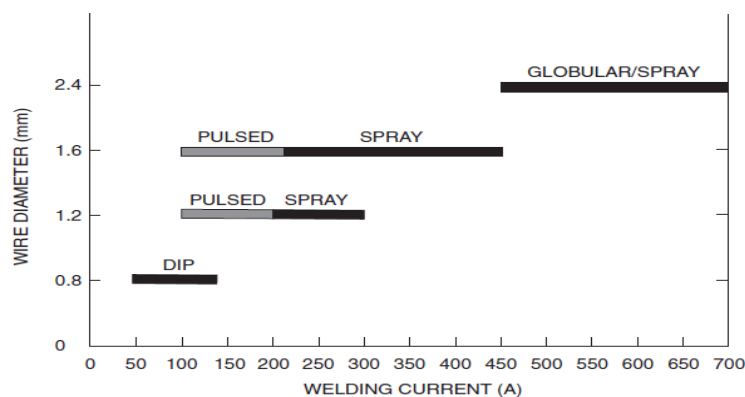


Fig 3.4. Typical welding current ranges for wire diameter and welding current.

Behaviour of metal transfer affecting the energy distribution in welding, as discussed in case of preparation of weld and bead on plate weld deposition [27], dictated by the pulse parameters. Generally two kinds of metal transfer, such as one droplet detachment per pulse and multiple droplets detachment per pulse are considered in P-GMAW process by keeping the pulse current at just above [31] and far higher than the transition current respectively. The transition current is defined by the current shifting the behavior of metal transfer [30] from the gravitational to spray mode.

With CO₂ shielding, the globular and non-axial, whatever may be the value of the welding current, current density and other factors. Hence there is considerable spatter. Drops become smaller in size as the current increases and they continue to be directed axially and non-axially. Axial transfer means that the metal droplets move along a line that is an extension of the longitudinal axis of the electrode. Non-axial transfer means that the droplets are hurled in any other directions. The non-axial transfer is caused by electromagnetic repulsive force acting on the bottom of the molten drop. The electric current flowing through the electrode gives rise to several electromagnetic forces that act on the metal tip including the pinch force (p) and the anode reaction force (R). The pinch force which increases with current and electrode diameter causes the drop to detach. With CO₂ shielding, the electrode tip is not heated directly by the arc plasma but by the arc heat conducted through the molten drop. The molten drop grows in size and finally detaches by short circuiting or gravity, after having overcome the force R , which tends to support the drop.

3.1.4 SELECTION AND DESIGN OF WELDS

In the design process, the goal is to produce a product that satisfies all requirements at the lowest cost. Welding is a vital approach in design because it is arguably the best joining process. The main processes for joining materials are fastening, welding, and casting. However, welding is still less expensive than casting and it is a more flexible. Welding is 3 to 4 times stronger than other processes so much less total material is required. It is also stiffer, has greater ductility, and is less likely to crack than castings. Lastly, welding resists impact loads better than castings [22].

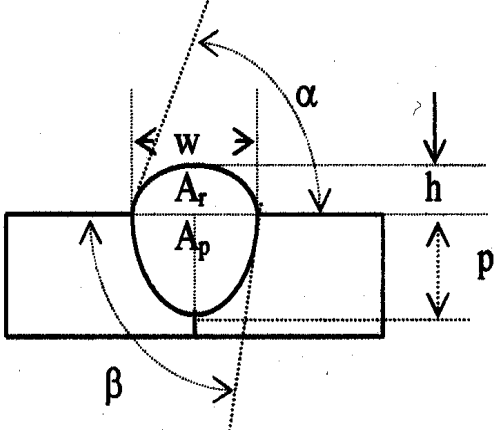
When welding is the selected design process the first step is to choose the type of joint used. To choose, the orientation, function, and loading must be determined. The section titled "Types of Joints" is a good reference to help determine what type of joint should be used. Once the type of joint is selected, the size, number, and locations of the welds must be determined. The information above and the section titled "Selecting Joint Design" are good references to help determine this.

Economics is another important design consideration. The design should be just above the requirements for strength and rigidity, including the factor of safety. The factor of safety should be large enough for contingencies, but not excessively large. Lastly, as in all other areas of machine design, using standardized components always is a good choice [22].

3.1.5 WELD BEAD GEOMETRY

The mechanical properties of the welded joints greatly depend on weld bead geometry, which in turn, is influenced by welding parameters like arc current, arc voltage, and arc travel speed. The bead geometry is specified by weld bead width, reinforcement height, reinforcement area, penetration height, penetration area and the contact angle of weld bead etc.

Table 3.1 Bead geometry

 $\%D = \frac{A_p}{A_t} 100 = \% \text{ dilution}$	A _p	Area of penetration
	A _r	Area of reinforcement
	α	Angle of convexity
	β	Angle of entry
	A _t	A _p + A _r Total weld bead area

The Weld Bead Width is the maximum width of the weld metal deposited. It increases with arc current, arc voltage; electrode weaving and decreases as arc travel speed increases. Penetration Height or simply penetration is the distance from base plate top surface to the maximum extent of the weld nugget. Penetration determines the load carrying capacity of a welded structure. Penetration Area is that covered by the fusion

line below the base metal level. Penetration area affects the weld strength. Reinforcement Height is the maximum distance between the base metal level and the top point of the deposited metal. Reinforcement Area is one included between the contour line of the deposited metal above the base metal level.

3.1.6 STAINLESS STEEL & WELDING

Iron and the most common iron alloy, steel, are from a corrosion viewpoint relatively poor materials since they rust in air, corrode in acids and scale in furnace atmospheres. In spite of this there is a group of iron-base alloys, the iron-chromium-nickel alloys known as *stainless steels*, which do not rust in sea water, are resistant to concentrated acids and which do not scale at temperatures up to 1100°C. Stainless steels are selected primarily because of their corrosion resistance, with the mechanical properties (strength, hardness, ductility) being of secondary importance. Stainless steels contain greater than 10.5 to 12 wt-% chromium, which provides a passive chromium oxide layer that forms on the surfaces when exposed to air or other oxidizing environments. As such, it is important when welding stainless steels that the weld metal be protected from sources of contamination or oxidation. Cleanliness is essential in welding stainless steels.

Types of Stainless Steels

There are five basic types of stainless steels:

- Austenitic (200 and 300 Series)
- Ferritic (some of the 400 Series)
- Martensitic (balance of the 400 Series)
- Precipitation hardening

The chemical compositions of some typical stainless steels are provided in Table 3.2. The first three types are classified according to the metallurgical structure they develop at room temperature. The majority of stainless steels are the austenitic 300 series, which contain chromium and nickel along with other alloying elements. These are nonmagnetic, have good toughness and ductility at elevated and low temperatures, and have the best general corrosion resistance of all stainless steels.

Austenitic stainless steels are iron-chromium-nickel alloys which are hardenable only by cold working. Nickel is the main element varied within the alloys of this class while carbon is kept to low levels. The nickel content may be varied from about 4% to 22% - higher values of nickel are added to increase the ductility of the metal. When chromium is increased to raise the corrosion resistance of the metal, nickel must also be increased to maintain the austenitic structure.

The ferritic stainless steels are ferromagnetic and have better resistance to stress-corrosion cracking, pitting, and crevice corrosion than the austenitics. The martensitics contain higher levels of carbon, which gives them very high strength. The duplex stainless steels contain two metallurgical phases at room temperature (austenite and ferrite), and thus they have some of the best properties of each. The precipitation-hardening stainless steels have other elements added (such as titanium) to form precipitates during a postweld heat treatment. These alloys can develop extremely high strengths

Table 3.2 **Typical Analysis in Percent:** [27]

<u>Type #</u>	<u>UNS #</u>	<u>C</u>	<u>Cr</u>	<u>Ni</u>	<u>Mn</u>	<u>Si</u>	<u>S</u>	<u>P</u>	<u>Mo</u>
302	S30200	.15	17-19	8-10	2.0	1.0	.03	.04	
304	S30400	.08	18-20	8-12	2.0	1.0	.03	.04	
304L	S30403	.03	18-20	8-12	2.0	1.0	.03	.04	
316	S31600	.08	16-18	10-14	2.0	1.0	.03	.04	2.0-3.0
316L	S31603	.03	16-18	10-14	2.0	1.0	.03	.04	2.0-3.0

(Percent maximum unless stated as a range or minimum.)

Table 3.3 **Typical Physical Properties:** [27]

<u>Type #</u>	<u>Density</u> <u>lb/in³</u>	<u>Specific Heat</u> <u>BTU/°F/lb</u> <u>0-100 °C</u>	<u>Thermal</u> <u>Conductivity</u> <u>BTU/Ft²/Ft/Hr/°F</u> <u>100 °C</u>	<u>Coefficient of</u> <u>Thermal Expansion</u> <u>Per °F x 10⁻⁶</u> <u>0-100 °C</u>	<u>Electrical</u> <u>Resistivity</u> <u>Microhm-cm</u> <u>21 °C</u>	<u>Magnetic</u> <u>Permeability</u> <u>(Annealed)</u> <u>μ</u>
302	.29	.12	9.4	9.6	72.0	1.008
304	.29	.12	9.4	9.6	70.0	1.008
304L	.29	.12	9.4	9.6	70.0	1.008
316	.29	.12	9.4	8.9	74.0	1.008
316L	.29	.12	9.4	8.9	74.0	1.008

Table 3.4 **Typical Mechanical Properties:**[27]

<u>(Annealed Cond.)</u> <u>Type #</u>	<u>Tensile Strength</u> <u>1000 Psi</u>	<u>Yield Strength</u> <u>1000 Psi</u>	<u>Elongation in</u> <u>2 inches. %</u>	<u>Reduction of</u> <u>Area. %</u>	<u>Brinell</u> <u>Hardness</u>
302	90	40	55	70	150
304	85	35	55	70	150
304L	80	30	55	70	140
316	85	35	60	70	150
316L	78	30	55	65	145

3.1.7 SHIELDING GASES

The quality, efficiency, and overall operating acceptance of the welding operation are strongly dependent on the shielding gas, since it dominates the mode of the metal transfer [1]. The shielding gas not only affects the properties of the weld but also determines the shape and penetration pattern [2]. It was found that the variation in the shielding gas composition causes some changes in microstructure and weld shape [4]. Some works have studied the influence of shielding gas composition on the apparent weld shape [5] on the surface tension of droplet that is traveling between electrode tip and weld pool and on the mode of the droplet transfer and the amount of resulting fume. It was found that small amount of oxygen added to the argon, improves the apparent shape and the droplet transfer mode [3, 8]. Since the carbon dioxide is an inexpensive shielding gas, it is added to the argon instead of oxygen.

Influence of the Shielding Gas on: GMAW

The choice of shielding gas has a significant influence on the following factors:

- Shielding Efficiency (Controlled shielding gas atmosphere)
- Metallurgy, Mechanical Properties (Loss of alloying elements, pickup of atmospheric gases)
- Corrosion Resistance (Loss of alloying elements, pickup of atmospheric gases)
- Weld Geometry (Bead and penetration profiles)
- Surface Appearance (Oxidation, spatters)
- Arc Stability and Ignition
- Environment (Emission of fumes and gases)

3.2 Weld metallurgy

3.2.1 Introduction

Welding metallurgy may be defined as the changes that occur in metals as a result of being joined by the welding process. These changes are manifested by changes in mechanical properties. Whenever we begin a discussion about metallurgy, we try to find out the changes brought about in the microstructure of the base metal and hence the changes in the mechanical properties of the base metal, a result of the welding [35]. In welding metallurgy, we are concerned with the time the material is at an elevated temperature and the rate at which the heat energy is applied to the base during welding as well as the rate at which the heat energy is removed during cooling after welding.

3.2.2 Weld pool solidification

Most knowledge of weld pool solidification is derived from the extrapolation of the knowledge of freezing of castings, ingots, and single crystals at lower thermal gradients and slower growth rates. Therefore, parameters important in determining microstructures in casting, such as growth rate (R), temperature gradient (G), undercooling (δT), and alloy composition determine the development of microstructures in welds as well. However, microstructure development in the weld zone is more complicated because of physical processes that occur due to the interaction of the heat source with the metal during welding, including re-melting, heat and fluid flow, vaporization, dissolution of gasses, solidification, subsequent solid-state transformation, stresses, and distortion. These processes and their interactions profoundly affect weld pool solidification and microstructure. During welding, where the molten pool is moved

through the material, the growth rate and temperature gradient vary considerably across the weld pool. Along the fusion line the growth rate is low while the temperature gradient is steepest. As the weld centerline is approached, the growth rate increases while the temperature gradient decreases. Consequently, the microstructure that develops varies noticeably from the edge to the centreline of the weld. In welds, weld pool solidification often occurs spontaneously by epitaxial growth on the partially melted grains. Since solidification of the weld metal proceeds spontaneously by epitaxial growth of the partially melted grains in the base metal, the weld zone grain structure is mainly determined by the base metal grain structure and the welding conditions. Crystallographic effects will influence grain growth by favouring growth along particular crystallographic directions, namely the easy growth directions. Conditions for growth are optimum when one of the easy growth directions coincides with the heat-flow direction. Thus, among the randomly oriented grains in a polycrystalline specimen, those grains that have one of their easy growth crystallographic axes closely aligned with heat-flow direction will grow at the expense of their neighbouring less favourably oriented grains. This is called competitive growth. Without additional nucleation, this will promote a columnar grain structure. Low values of $G/(R)^{1/2}$ indicate as increased tendency to constitutional super cooling thus favouring the dendritic mode of solidification. On the other hand steep temperature gradients in the liquid and slow growth rates favour cellular growth.

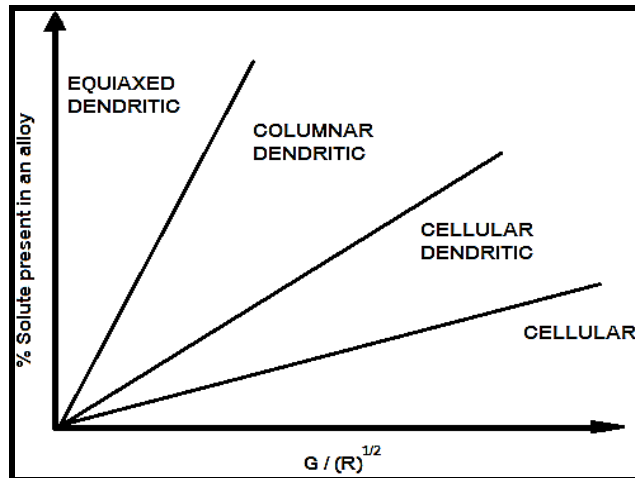


Figure 3.5: influence of grain growth rate R and temperature gradient G, on the pattern of solidification[35]

3.2.3 Zones in a weld

If one looks closely at macrostructure of the weld zone he can clearly identify three distinct zones:

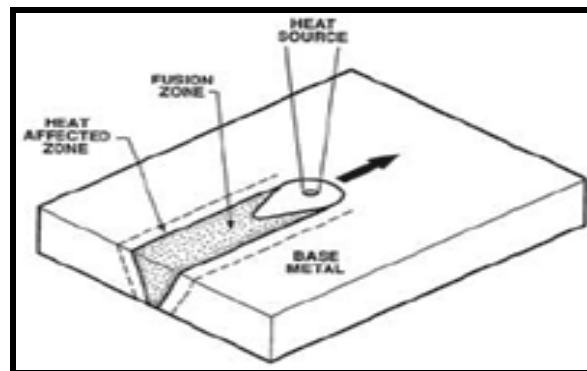


Figure 3.6: Regions in a weldments[35]

Weld metal zone:

Weld metal zone is formed as the weld metal solidifies from the molten state. This is a mixture of parent metal, electrode, filler metal; the ratio depending upon the welding process used, the type of joint plate thickness. Weld metal zone is a cast metal of particular composition of mixture that has cooled; its microstructure reflects the

cooling rate in the weld. Depending upon the chemical composition a martensitic structure in the weld indicates a very high cooling rate; fine pearlite and coarse pearlite shows comparatively slower cooling rates. From the molten weld pool the first metal solidifies epitaxially upon the solid grains of the un-melted base metal.

Depending upon the composition and solidification rates the weld solidifies in a cellular or dendritic growth mode. Both modes cause segregation of alloying elements and consequently the weld metal is less homogeneous on the micro level than the base metal and therefore cannot be expected to have the same properties as wrought parent metal unless the filler metal in the as deposited condition has same properties as that of parent metal.

Heat Affected Zone:

It consists of parent metal that did not melt but was heated to high enough temperature for a sufficient period of time that grain growth occurred and mechanical as well as microstructural properties have been altered by the heat of welding. The HAZ is subjected to complex thermal cycle in which all temperatures from the melting range of the steel down to comparatively much lower temperatures are involved. HAZ usually consists of a variety of microstructures. These structures may range from very narrow regions of hard martensite to coarse pearlite. This renders HAZ the weakest area in weld. Except where there are obvious defects in the weld deposit, most welding failures originate in the HAZ. In GMAW the HAZ consists of 3 sub zones

- a. Grain growth region: It is immediately adjacent to the weld metal zone. In this zone the parent metal has been heated well above the upper critical temperature,

this resulted in grain growth or coarsening of the structure. The maximum grain size and extent of this region increases as the cooling rate decreases.

- b. Grain refined region: The refined zone indicates that in this region the parent metal has been heated to just above upper critical temperature where grain refinement is complete and finest grain structure exists. Complete recrystallization has taken place in this zone
- c. Transition zone: Temperature exists between upper and lower recrystallization temperature where partial allotropic recrystallization takes place.

Unaffected parent metal: Outside the HAZ is the base metal which was not affected by the thermal cycles during welding.

3.3 Response Surface Methodology (RSM)

3.3.1 Introduction

The Response Surface Methodology (RSM) is a collection of mathematical and statistical techniques useful for the modeling and analysis of problems in which a response of interest is influenced by several variables and the objective is to optimize this response. The most extensive application of RSM is particularly in situations where several input variables potentially influence some performance measure or quality characteristic of the product or process. This performance measure or quality characteristic is called Response. It is typically measured on a continuous scale. Most of the real world application of RSM will involve more than one response. The input variables are sometimes called independent variables and they are subject to the control of the engineer or scientist, at least for the purpose of a test or an experiment.

In most *RSM* problems, the true response function f is unknown. In order to develop a proper approximation for f , the experimenter usually starts with a low-order polynomial in some small region. If the response can be defined by a linear function of independent variables, then the approximating function is a first-order model. A first-order model with 2 independent variables can be expressed as

$$y = b_0 + b_1x_1 + b_2x_2 + e$$

If there is a curvature in the response surface, then a higher degree polynomial should be used. The approximating function with 2 variables is called a second-order model:

$$y = b_0 + b_1 + b_2 + b_{11}x_{11}^2 + b_{22}x_{22}^2 + b_{12}x_{12} + e$$

In general all *RSM* problems use either one or the mixture of the both of these models. In order to get the most efficient result in the approximation of polynomials the proper experimental design must be used to collect data. Once the data are collected, the *Method of Least Square* is used to estimate the parameters in the polynomials. The response surface analysis is performed by using the fitted surface. The response surface designs are types of designs for fitting response surface.

3.3.2 Central Composite Design

A Box-Wilson Central Composite Design commonly called 'a central composite design,' contains an imbedded factorial or fractional factorial design with centre points that is augmented with a group of 'star points' that allow estimation of curvature. If the distance from the centre of the design space to a factorial point is ± 1 unit for each factor, the distance from the centre of the design space to a star point is $\pm\alpha$ with $|\alpha| > 1$. The precise value of α depends on certain properties desired for the design and on

the number of factors involved. Similarly, the number of centre point runs the design is to contain also depends on certain properties required for the design.

3.4 Experimentation

The main aim of the project was to investigate and statistical analysis of process variables on the bead geometry of Synergic MIG Welding and to develop mathematical models to describe the relationship between the input and output variables. Metallurgical analysis was also done to co-relate the effects of input parameters on the microhardness and the micro structure of the welded specimen. To achieve the above mentioned objectives, following are the sequence of steps which were carried out:

1. Identification of important process control variables
2. Deciding the working range of the process control variables, viz. Welding Current(A), plate thickness(T), gas flow rate(G) and Travel Speed (S)
3. Developing the design matrix
4. Conducting the experiments as per the design matrix
5. Recording the responses viz. bead height (H), bead width (W) and bead penetration (P)
6. Developing the mathematical models
7. Checking the adequacy of the models
8. Finding the significance of co-efficient
9. Developing the final proposed models
10. Plotting of graphs and drawing conclusions
11. Finding the micro hardness and micro structure

12. Metallurgical analysis to co-relate the micro hardness and the micro structure of the welded material with the process variables

13. Discussion of the results

3.4.1 Identification of important process control variables

Based on the effect on weld bead geometry, ease of control and capability of being maintained at the desired level, four independently controllable process parameters were identified namely, the welding current (A); the travel speed (S), gas flow rate(R) and the plate thickness (T) at constant nozzle to plate distance. The weld bead geometry parameters chosen for this study were bead height (H), bead width (W) and bead penetration (P).

3.4.2 Selection of design parameters

Trial runs were conducted by varying the process parameters at a time. The working range was fixed by previous research papers. The upper and lower limits were coded as +2 and -2, respectively. The coded values for intermediate values can be calculated from the relationship:

$$X_i = \frac{2[2X - (X_{\max} + X_{\min})]}{(X_{\max} - X_{\min})}$$

Where, X_i is the required coded value of a variable X , when X is any value of the variable from X_{\min} to X_{\max} ; X_{\max} and X_{\min} are the maximum and minimum levels of the variables. The selected process parameters and their upper and lower limits together with notations and units are given in Table 3.5.

Table 3.5: Design parameters and their limits

PARAMETERS USED	LEVELS				
	1 (-2)	2 (-1)	3 (0)	4 (1)	5 (2)
Plate thickness(mm)	3	6	8	12	15
Gas flow rate (lit/min.)	8	10	13	15	18
Current (A)	166	200	241	275	316
Travel speed (cm/min.)	27	32	37	42	47

3.4.3 Developing the design of experiment

A fully rotatable 4 factor 5 level central composite design matrix was used for the experiment. To maintain rotatability the value of α is chosen as 2. A fully rotatable central composite design matrix covers greater design space than the factorial design matrix, thus resulting in greater accuracy of the established relationships. Table 3.4 shows the 30 sets of coded conditions used to form the design matrix. The first 16 conditions have been formulated as per 2^4 (two levels and 4 factors) factorial design. These factorial points represents the variance optimal design for a first order or first order plus 2 factor interaction model. The next eight experimental conditions are called as Star points, i.e. keeping one factor at the lowest/highest level and the remaining factors at middle level. Addition of Star points allow for efficient estimation of pure quadratic terms in case of existence of curvature in the system. Curvature is an indication of presence of interaction between 2 or more variables. The last six

experimental conditions are known as centre points i.e., keeping all the factors at the middle level and it is normally done to know the repeatability of the experimental procedures. Centre points provide information about the existence of curvature in the system. Thus the 30 experimental runs allowed the estimation of the linear, quadratic and the two way interactive effects of the welding variables on the bead geometry and provide results with greater accuracy while dealing with large number of factors.

Table 3.6 coded values

Run order	Standard order	Blocks	Plate thickness	GFR	Travel speed	Current
1	03	1	-1	1	-1	-1
2	24	1	0	0	0	2
3	16	1	1	1	1	1
4	29	1	0	0	0	0
5	04	1	1	1	-1	-1
6	21	1	0	0	-2	0
7	01	1	-1	-1	-1	-1
8	10	1	1	-1	-1	1
9	05	1	-1	-1	1	-1
10	28	1	0	0	0	0
11	08	1	1	1	1	-1
12	11	1	-1	1	-1	1
13	23	1	0	0	0	-2
14	22	1	0	0	2	0
15	02	1	1	-1	-1	-1
16	26	1	0	0	0	0
17	12	1	1	1	-1	1
18	30	1	0	0	0	0
19	15	1	-1	1	1	1

20	18	1	2	0	0	0
21	27	1	0	0	0	0
22	14	1	1	-1	1	1
23	19	1	0	-2	0	0
24	25	1	0	0	0	0
25	06	1	1	-1	1	-1
26	20	1	0	2	0	0
27	09	1	-1	-1	-1	1
28	07	1	-1	1	1	-1
29	13	1	-1	-1	1	1
30	17	1	-2	0	0	0

Table 3.7 Actual Values

Run order	Standard order	Blocks	Plate thickness	GFR	Travel speed	Current
1	03	1	6	15	32	200
2	24	1	8	13	37	136
3	16	1	12	15	42	275
4	29	1	8	13	37	241
5	04	1	12	15	32	200
6	21	1	8	13	27	241
7	01	1	6	10	32	200
8	10	1	8	10	32	275
9	05	1	6	10	42	200
10	28	1	8	13	37	241
11	08	1	12	15	42	200
12	11	1	6	15	32	275
13	23	1	8	13	37	166

14	22	1	8	13	47	241
15	02	1	12	10	32	200
16	26	1	8	13	37	241
17	12	1	12	15	32	275
18	30	1	8	13	37	241
19	15	1	6	15	42	275
20	18	1	15	13	37	241
21	27	1	8	13	37	241
22	14	1	12	10	42	275
23	19	1	8	8	37	241
24	25	1	8	13	37	241
25	06	1	12	10	42	200
26	20	1	8	18	37	241
27	09	1	6	10	32	275
28	07	1	6	15	42	200
29	13	1	6	10	42	241
30	17	1	3	13	37	241

3.4.4 Experimental set up

Power sources

The Synergic MIG arc requires a power source that will provide direct current and with a suitable relationship established between welding current and voltage, this relationship being known as the *power source dynamic characteristic*. As mentioned above the MIG process uses a continuous wire feed and for the majority of welding operations it is important that the rate at which the wire burns off in the arc is matched by the wire feed speed. Failure to do this can result in an unstable arc and variable weld

quality. To achieve this control many SMIG/MAG welding power sources are designed with a *flat* or *constant voltage* characteristic.

The importance of this characteristic becomes apparent when we consider what happens during manual welding. The manual welder cannot maintain a fixed invariable arc length while welding an unsteady hand or repositioning himself during welding means that the arc length varies and this in its turn causes variations in arc voltage. When this happens with a flat characteristic power source a small increase in the arc length results in an increase in arc voltage, giving a large drop in arc current, as illustrated in Fig.3.7. Since the wire burn-off rate is determined by the current this also decreases, the tip of the wire moves closer to the weld pool, decreasing the voltage and raising the current as it does so. The burn-off rate therefore rises, the arc length increases and we have what is termed a *self-adjusting arc* where a constant arc length and filler metal deposition rate are maintained almost irrespective of the torch movement.

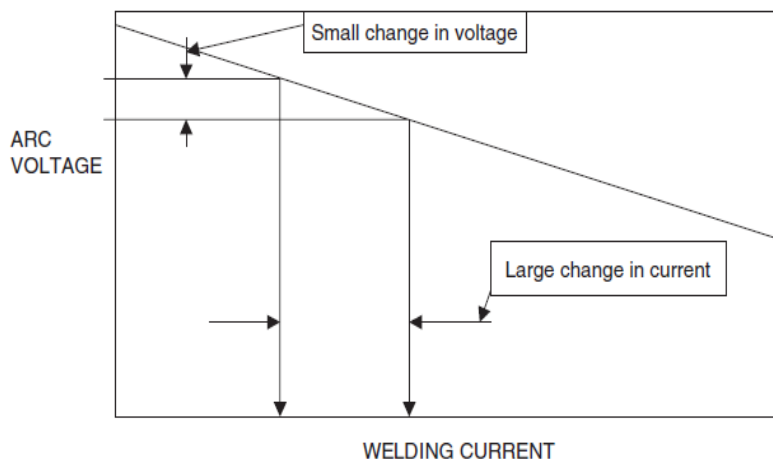


Fig 3.7 Schematic of the effect of arc voltage Vs arc current. Flat characteristic power source [2]

During both dip and spray transfer the speed at which the power source responds to the changes in the arc length is determined by the inductance in the welding circuit. This controls the rate of current rise or fall and can have a significant effect on weld quality. Insufficient inductance permits the welding current to rise extremely rapidly, giving rise to excessive spatter and burning back of the wire to the contact tip. Too high an inductance means that the wire does not melt sufficiently rapidly and the wire tip may stub into the weld pool or be pushed through the root pass to protrude from the root. It is essential therefore that the power source is adjusted for the correct amount of inductance when, for example, the wire diameter or wire feed speed is changed.

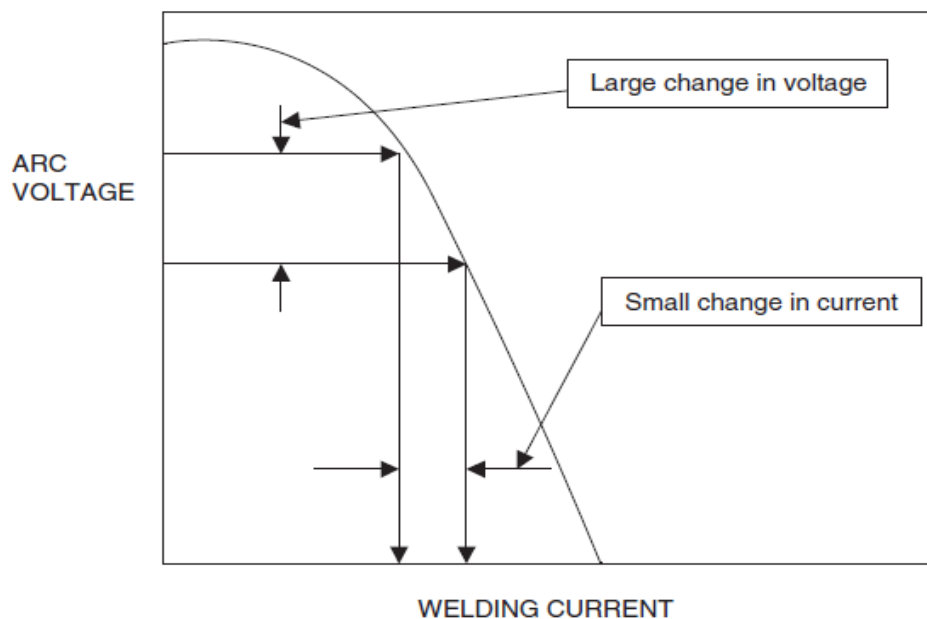


Fig 3.8. Schematic of effect of arc voltage vs arc current. Drooping characteristic power source.[2]



Fig3.9. Experimental set up for Synergic MIG Welding

The converse of the flat characteristic power source is the *drooping characteristic* or *constant current* power source, illustrated in Fig.6 with a drooping characteristic a large change in arc voltage results in only a small change in arc current. Heat input is therefore reasonably constant, unlike that from a flat characteristic power source arc, giving more consistent penetration

3.4 .5 EXPERIMENTAL PROCEDURE

Bead on plate technique was employed for depositing the weld beads on stainless steel plate (304L) using semi mechanized welding station. For the experiment, five different parameters were taken; they are plate thickness, gas flow rate, Travel speed, and current. By using RSM technique, 30 run orders were computed for five

different levels. Correspondingly 30 plates were cut each of dimensions 6 inch in length of five different thicknesses:

Table 3.8 Distribution of plate thickness

Thickness (mm)	No. of plates
3	01
6	08
8	13
12	07
15	01



Fig.3.10. welded plates

After cutting all plates, welding was carried out as per specified parameters for all plates individually. In the welding experiment, a 304L filler wire with a 1.2 mm diameter was used. All experiments were carried out with a contact-tip to work distance of 20 mm using the mixture of Argon and CO₂ as shielded gas at five different flow rates. A Direct current power source was used to perform the bead on plate by means of synergic MIG process. The experimental setup is shown in figure 3.9 and the welded pieces are shown in figure 3.10.

3.5 Observation of the experiment:

The observed values of bead profile, voltage transient and other parameters are in the table form for all 30 runs. First six observations are given below and others are in appendix.

Table 3.9 observation1

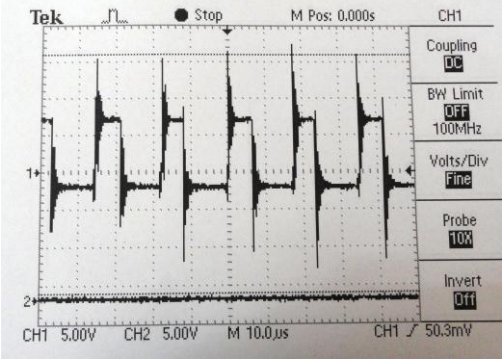

V		T	G	I	S	V	Weld bead
		6	10	200	32	21.1	
		H		W		P	
		3.16		7.44		2.11	

Table 3.10 observation2

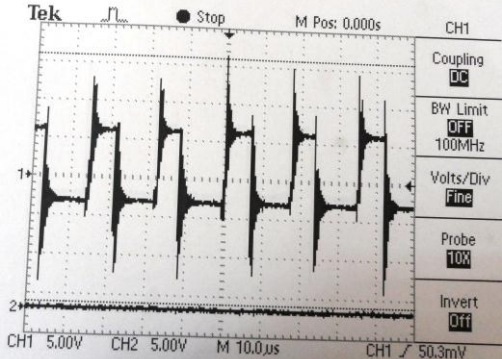

V		T	G	I	S	V	Weld bead
		12	10	200	32	17.7	
		H		W		P	
		3.35		10.22		2.45	

Table 3.11 observation3

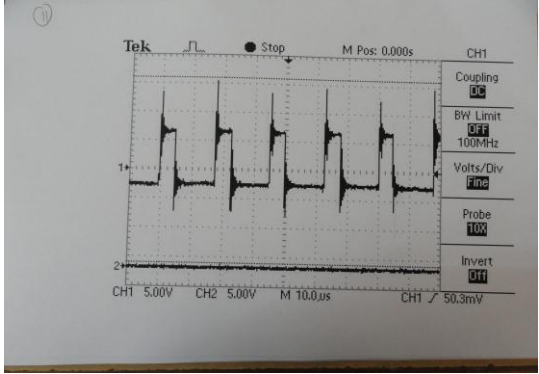

V		T	G	I	S	V	Weld bead	
		5	15	200	32	20.8		
		H		W		P		
		3.56		8.14		1.96		

Table 3.12 observation4

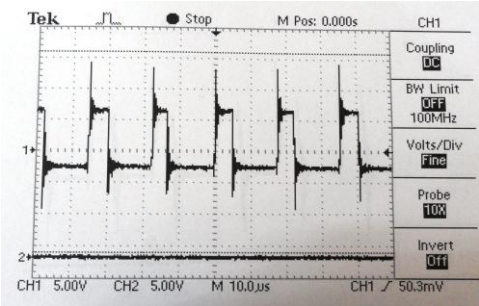

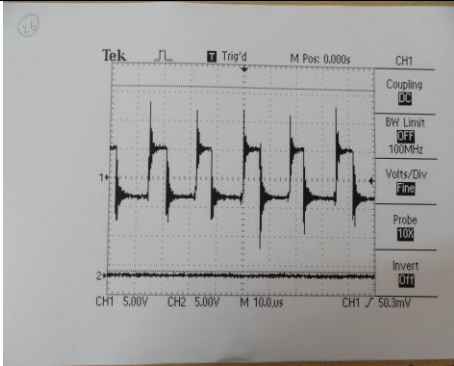

V		T	G	I	S	V	Weld bead	
		12	15	200	32	25.1		
		H		W		P		
		3.10		8.85		2.48		

Table 3.13 observation 5

V		T	G	I	S	V	Weld bead	
		6	10	200	42	21.1		
		H		W		P		
		2.86		6.95		1.46		

3.6 Sample preparation for bead measurement

This procedure of preparation of a specimen involves the method of preparing the samples cut out from the plates fit for viewing under a metallurgical microscope. The ultimate objective is to produce a flat, scratch free, mirror like surface. The steps involved in our specimen preparation are as follows

a) Sampling: – The choice of a sample for microscopic study may be very important. If a failure is to be investigated, the sample should be chosen as close as possible to the area of failure and should be compared with one taken from the normal section. If the material is soft as non-ferrous metals and alloys and non-heat treated steels, the section may be obtained by manual hack sawing. If the material is hard, the section may be obtained by use of an abrasive cutoff wheel. In our case it was stainless steel hence used grinding wheel for cutting the samples.

b) Rough grinding: – Whenever possible, the specimen should be of a size that is convenient to handle. Our sample is made flat by slowly moving it up and back across the surface of a flat smooth file. Specimen is made rough ground on a belt sander, with the specimen kept cool by frequent dropping in water during grinding operation. The rough grinding is continued until the surface is flat and free of nicks, burrs, etc., and all scratches due to the hacksaw or cutoff wheel are no longer visible.

c) Intermediate polishing or grinding: - Grinding is done using rotating discs covered with silicon carbide paper and water. There are a number of grades of paper, with 180, 240, 400, 1000, grains of silicon carbide per square inch. 180 grades therefore represent the coarsest particles and this is the grade to begin the grinding operation. Always use light pressure applied at the center of the sample. Continue grinding until all

the blemishes have been removed, the sample surface is flat, and all the scratches are in a single orientation. Wash the sample in water and move to the next grade, orienting the scratches from the previous grade normal to the rotation direction. This makes it easy to see when the coarser scratches have all been removed. After the final grinding operation on 1000 paper, the sample is washed in water followed by acetone and dried before moving to the polishers.

d) Fine polishing: - The polishers consist of rotating discs covered with soft cloth impregnated with diamond particles (1 and 0.5 micron size) and an oily lubricant. It began with the 1 micron grade and polishing continued until the grinding scratches have been removed. It is of vital importance that the sample is thoroughly cleaned using soapy water, followed by acetone, and dried before moving onto the final 0.5 micron stage. A properly polished sample showed only the nonmetallic inclusions and will be scratch free

e) Etching: - The purpose of etching is two-fold. Grinding and polishing operations produce a highly deformed, thin layer on the surface which is removed chemically during etching. Secondly, the etchant attacks the surface with preference for those sites with the highest energy, leading to surface relief which allows different crystal orientations, grain boundaries, precipitates, phases and defects to be distinguished in reflected light microscopy. There are many tried and tested etchants available but there are mandatory safety issues associated with the preparation and use of all of these. The selection of the appropriate etching reagent is determined by the metal or alloy and the specific structure desired for viewing. In this case I used ferric chloride and hydrochloric

acid etching reagent. Its composition is ferric chloride (5g), hydrochloric acid (50ml), and water (10ml). And in this case the etching time is a few seconds to 1 min.



Fig.3.11 samples after etching



Fig.3.12 bead geometry after etching

Table 3.39 Recording of responses

Weld No.	Input parameters				Responses		
	T	G	S	I	Bead height (H)	Bead width (W)	Bead Penetration (P)
1	-1	-1	-1	-1	3.16	7.44	2.11
2	+1	-1	-1	-1	3.35	10.22	2.45

3	-1	+1	-1	-1	3.56	8.14	1.96
4	+1	+1	-1	-1	3.1	8.85	2.48
5	-1	-1	+1	-1	2.86	6.95	1.46
6	+1	-1	+1	-1	3.17	8.08	1.62
7	-1	+1	+1	-1	3.63	6.98	1.63
8	+1	+1	+1	-1	3.3	6.59	1.63
9	-1	-1	-1	+1	3.71	8.16	2.15
10	+1	-1	-1	+1	3.58	10.02	2.18
11	-1	+1	-1	+1	3.74	6.55	1.72
12	+1	+1	-1	+1	2.93	6.92	1.86
13	-1	-1	+1	+1	3.51	9.33	2.13
14	+1	-1	+1	+1	3.5	10.18	1.89
15	-1	+1	+1	+1	3.78	7.56	1.98
16	+1	+1	+1	+1	3.13	6.92	2.04
17	-2	0	0	0	3.59	7.76	1.99
18	+2	0	0	0	3.16	8.69	2.26
19	0	-2	0	0	3.26	10.12	2.27
20	0	+2	0	0	3.38	7.02	2.12
21	0	0	-2	0	3.35	8.7	2.05
22	0	0	+2	0	3.23	7.79	1.9
23	0	0	0	-2	3.28	7.28	1.76
24	0	0	0	+2	3.78	7.81	1.82
25	0	0	0	0	3.47	7.71	1.89
26	0	0	0	0	3.44	7.79	1.91
27	0	0	0	0	3.47	7.78	1.9
28	0	0	0	0	3.46	7.52	1.93
29	0	0	0	0	3.52	7.73	1.92
30	0	0	0	0	3.45	7.78	1.89

CHAPTER 4

DEVELOPMENT OF MATHEMATICAL MODELS

The regression coefficients were calculated with the help of statistical software, Design-Expert 8.5.0 and the adequacy of the model was tested by using the analysis of variance technique (ANOVA). The experimental data were used to develop nonlinear models, and analysis of the models was carried out through ANOVA and surface plots.

Table 4.1 Design Summary

responce	Units	Obs	Analysis	Min.	Max.	Mean	Std Dev.	Ratio	Model
H	mm	30	polynomial	2.86	3.78	3.395	0.2365	1.321	Quadratic
W	mm	30	polynomial	6.55	10.22	8.020	1.0716	1.560	Quadratic
P	mm	30	polynomial	1.46	2.48	1.957	0.2460	1.698	Quadratic

4.1 Checking adequacy of the model

The analysis of variance (ANOVA) technique was used to check the adequacy of the developed models. As per this technique:

- (a) The F-ratio of the developed model is calculated and is compared with the standard tabulated value of F-ratio for a specific level of confidence

(b) If calculated value of F-ratio does not exceed the tabulated value, then with the corresponding confidence probability the model may be considered adequate. For our analysis, we have taken a confidence interval of 95%.

4.1.1 Response: Reinforcement Height

Table 4.2.ANOVA for Reinforcement Height

Source	Sum of squares	D _f	Mean square	F value	p-value Prob> F
Model	1.61	14	0.12	146.07	<0.0001 (significant)
A-Plate thickness	0.32	1	0.32	128.23	<0.0001
B-GFR	0.014	1	0.014	18.39	0.0006
C-Travel speed	0.010	1	0.010	13.59	0.0022
D-Current	0.32	1	0.32	128.23	<0.0001
AB	0.43	1	0.43	157.27	<0.0001
AC	0.018	1	0.018	23.85	0.0002
AD	0.11	1	0.11	87.86	<0.0001
BC	0.10	1	0.10	78.65	<0.0001
BD	0.20	1	0.20	166.25	<0.0001
CD	0.51	1	0.51	187.21	0.0383
A ²	0.016	1	0.016	21.20	0.0003

B ²	0.039	1	0.039	52.69	<0.0001
C ²	0.056	1	0.056	63.25	<0.0001
D ²	6.086E-003	1	6.086E-003	8.27	0.0116
Residual	0.011	15	7.361E-004		
Lack of fit	7.158E-003	10	7.158E-004	0.92	0.5752(not significant)
Pure error	3.883E-003	5	7.767E-004		
Cor total	1.69	29			

The Model F-value of 146.07 implies the model is significant. There is only a 0.01% chance that a "Model F-Value" this large could occur due to noise. Values of "Prob > F" less than 0.0500 indicate model terms are significant. In this case A, B, C, D, AB, AC, AD, BC, BD, A², B², C², D² are significant model terms. Values greater than 0.1000 indicate the model terms are not significant. If there are many insignificant model terms (not counting those required to support hierarchy), model reduction may improve your model. The "Lack of Fit F-value" of 0.92 implies the Lack of Fit is not significant relative to the pure error. There is a 57.52% chance that a "Lack of Fit F-value" this large could occur due to noise. Non-significant lack of fit is good -- we want the model to fit.

The "Predicted R-Squared" of 0.9711 is in reasonable agreement with the "Adjusted R-Squared" of 0.9868. "Adeq Precision" measures the signal to noise ratio. A ratio

greater than 4 is desirable. In this case ratio of 49.345 indicates an adequate signal.

This model can be used to navigate the design space.

4.1.2 Response: Bead Width

Table 4.3. ANOVA for Bead Width

Source	Sum of squares	D _f	Mean square	F value	p-value Prob> F
Model	33.23	14	2.37	88.23	<0.0001 (significant)
A-Plate thickness	3.03	1	3.03	115.7	<0.0001
B-GFR	13.61	1	13.61	427.42	<0.0001
C-Travel speed	1.27	1	1.27	48.63	<0.0001
D-Current	0.50	1	0.50	18.93	<0.0006
AB	2.70	1	2.70	102.96	<0.0001
AC	1.42	1	1.42	54.27	<0.0001
AD	0.20	1	0.20	7.64	0.0145
BC	0.077	1	0.077	2.94	0.1073
BD	3.62	1	3.62	138.13	<0.0001
CD	4.40	1	4.40	167.9	<0.0001
A ²	0.34	1	0.34	13.04	0.0026

B ²	1.07	1	1.07	40.96	<0.0001
C ²	0.37	1	0.37	14.22	0.0018
D ²	0.094	1	0.094	3.57	0.0781
Residual	0.39	15	0.026		
Lack of fit	0.34	10	0.034	3.26	0.1022(not significant)
Pure error	0.052	5	0.010		
Cor total	32.98	29			

The Model F-value of 88.83 implies the model is significant. There is only a 0.01% chance that a "Model F-Value" this large could occur due to noise. Values of "Prob > F" less than 0.0500 indicate model terms are significant. In this case A, B, C, D, AB, AC, AD, BD, CD, A², B², C² are significant model terms. Values greater than 0.1000 indicate the model terms are not significant. The "Lack of Fit F-value" of 3.26 implies the Lack of Fit is not significant relative to the pure error. There is a 10.22% chance that a "Lack of Fit F-value" this large could occur due to noise. Non-significant lack of fit is good, we want the model to fit.

The "Predicted R-Squared" of 0.9382 is in reasonable agreement with the "Adjusted R-Squared" of 0.9770. "Adeq Precision" measures the signal to noise ratio. A ratio greater than 4 is desirable. Our ratio of 31.262 indicates an adequate signal.

4.1.3Response: Depth of Penetration

Table 4.4.ANOVA for Bead Width

Source	Sum of squares	D _f	Mean square	F value	p-value Prob> F
Model	1.74	14	0.12	143.76	<0.0001 (significant)
A-Plate thickness	0.13	1	0.13	155.97	<0.0001
B-GFR	0.023	1	0.023	26.36	0.0001
C-Travel speed	0.50	1	0.50	428.21	<0.0001
D-Current	9.600E-003	1	9.600E-003	11.09	0.0046
AB	0.029	1	0.029	33.39	<0.0001
AC	0.040	1	0.040	46.21	<0.0001
AD	0.10	1	0.10	118.31	<0.0001
BC	0.11	1	0.11	122.03	<0.0001
BD	0.070	1	0.070	81.13	<0.0001
CD	0.40	1	0.40	367.9	<0.0001
A ²	0.084	1	0.084	97.32	<0.0001
B ²	0.15	1	0.15	168.49	<0.0001
C ²	0.038	1	0.038	43.58	0.0018
D ²	0.022	1	0.022	25.44	.0001

Residual	0.013	15	8.656E-004		
Lack of fit	0.012	10	1.165E-003	4.37	0.0587(not significant)
Pure error	1.333E-003	5	2.667E-004		
Cor total	1.76	29			

The Model F-value of 143.76 implies the model is significant. There is only a 0.01% chance that a "Model F-Value" this large could occur due to noise. Values of "Prob > F" less than 0.0500 indicate model terms are significant. In this case A, B, C, D, AB, AC, AD, BC, BD, CD, A², B², C², D² are significant model terms. Values greater than 0.1000 indicate the model terms are not significant. If there are many insignificant model terms (not counting those required to support hierarchy), model reduction may improve your model. The "Lack of Fit F-value" of 4.37 implies there is a 5.87% chance that a "Lack of Fit F-value" this large could occur due to noise. Non-significant lack of fit is good, we want the model to fit.

The "Predicted R-Squared" of 0.9607 is in reasonable agreement with the "Adjusted R-Squared" of 0.9857. "Adeq Precision" measures the signal to noise ratio. A ratio greater than 4 is desirable. Our ratio of 47.749 indicates an adequate signal. This model can be used to navigate the design space.

The bead geometry parameters were expressed as a non –linear function of the input process parameters.

4.1.4 Final proposed models:

$$\begin{aligned} \text{reinforcement height} = & + 3.46833 - 0.11458(T) + 0.023750(G) - 0.020417(S) + \\ & 0.11458(I) - 0.16312(T*G) + 0.033125(T*S) - 0.08187(T*I) + 0.079375(G*S) - \\ & 0.11062(G*I) + 0.010625(S*I) - 0.023854T^2 - 0.037604G^2 - 0.045104S^2 + 0.014896(I)^2. \end{aligned}$$

$$\begin{aligned} \text{weld width} = & + 7.71833 + 0.38542 * T - 0.77042 * G - 0.24792 * S + 0.12625 * I - \\ & 0.38437T*G - 0.27187T *S - 0.08562T*I - 0.043125 G*S - 0.44937 G*I + 0.5506S*I + \\ & 0.098229T^2 + 0.20573G^2 + 0.12448S^2 - 0.050521(I)^2 \end{aligned}$$

$$\begin{aligned} \text{Depth of penetration} = & + 1.91 + 0.075 * T - 0.031*G - 0.14*S + 0.020*I + 0.043*T*G - \\ & 0.050 T*S - 0.080T*I + 0.081G*S - 0.066G*I + 0.16S*I + 0.055T^2 + 0.073G^2 - 0.037S^2 - \\ & 0.028I^2 \end{aligned}$$

4.1.5 Testing the models

The developed models were tested for the accuracy of their predictive ability. 5 test cases were selected at random from the design matrix and the experimental bead geometry parameters were compared to the parameters obtained from the mathematical models. The results are summarized in Table 4.5 below:

Table 4.5: Testing of mathematical model

Run order	Plate thickness	GFR	Travel speed	current		Actual value	Predicted value	% Error
07	6	15	42	200	H	3.63	3.58	1.37
					W	6.98	7.15	-2.43
					P	1.63	1.62	0.06

13	6	10	42	275	H	3.51	3.48	0.085
					W	9.33	9.42	-0.09
					P	2.13	2.02	5.16
18	15	13	37	241	H	3.16	3.13	0.095
					W	8.69	8.88	-2.18
					P	2.26	2.19	3.09
21	8	13	27	241	H	3.35	3.31	1.19
					W	8.70	8.65	0.057
					P	2.05	2.05	0
27	8	13	37	241	H	3.47	3.39	2.30
					W	7.78	7.62	2.05
					P	1.90	1.89	0.05

This table indicates that percentage of error in the mathematical model is very low.

Hence this model is good and can be used to predicting the weld parameters.

CHAPTER 5

RESULTS AND DISCUSSION

5.1 Effect of process parameters on metal transfer

With the use of oscilloscope, it is possible to observe the format of the current and voltage traces produced by welding processes. These signal waves may mimic some metal transfer modes. For instance, during short circuiting transfer, when the droplet is starting its development, voltage oscillates around a mean value but tends to zero when the drop touches the pool (short-circuit). A voltage peak happens just after the drop detachment, due to the arc reignition phenomenon.

Thus, it is possible to detect droplet detachment electrically by using a storage oscilloscope or transient recorder. The detachment generates a small blip on the arc voltage trace, probably due to the increased electrical resistance of the droplet neck just before separation. The technique presents here, showed to be suitable for welding metal transfer analysis and presented the following advantages over the traditional methods: it is possible to identify visually and to assort with precision the behavior of the welding electrical signals during the several phases of the metal transfer.

High current and high voltage produced the mixed mode but predominantly axial spray and occasional short circuiting transfer in between. The weld bead ripples were fairly uniform and the general appearances of the bead were very good. The results are concluded from the table 4.1 to 4.30.

5.2 Effects of process parameters on reinforcement height:

The reinforcement height varies from 2.86mm to 3.78mm. Figure 5.1 shows the relation between reinforcement height and welding parameters. Fig. 5.1(a) shows that as plate thickness increases, the reinforcement height is decreases. Reinforcement height increases as GFR increases. The reinforcement height decreases from 3.35mm to 2.86mm when travel speed increases from 27 to 47 cm/min. as plate thickness varies from 6 mm to 15 mm.

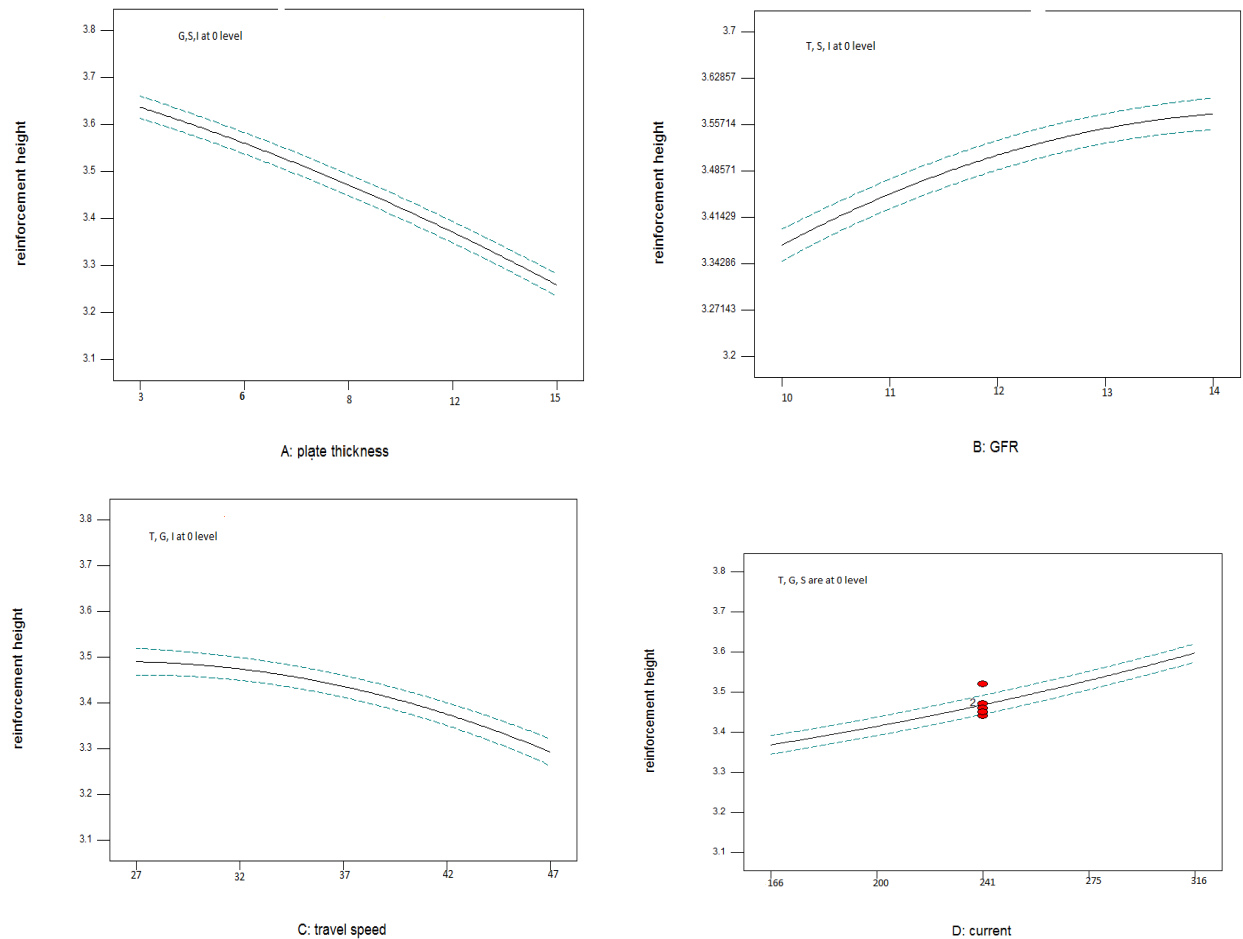


Figure5.1. (A) reinforcement height Vs plate thickness (B) reinforcement height Vs GFR(C) reinforcement height Vs Travel speed

(D) reinforcement height Vs current

This is because of the fact that when the welding torch travels at a greater speed over the base metal the line power per unit length of weld bead is reduced and also the welding torch covers more distance per unit time. The reinforcement height increased 3.36mm to 3.67mm when current was increased from low level to high level as shown in figure 5.1(d). This was due to the larger amount of metal deposited per unit length. The increased proportion of weld metal deposited with the increase in welding wire feed rate got distributed in the bead width and the height of reinforcement.

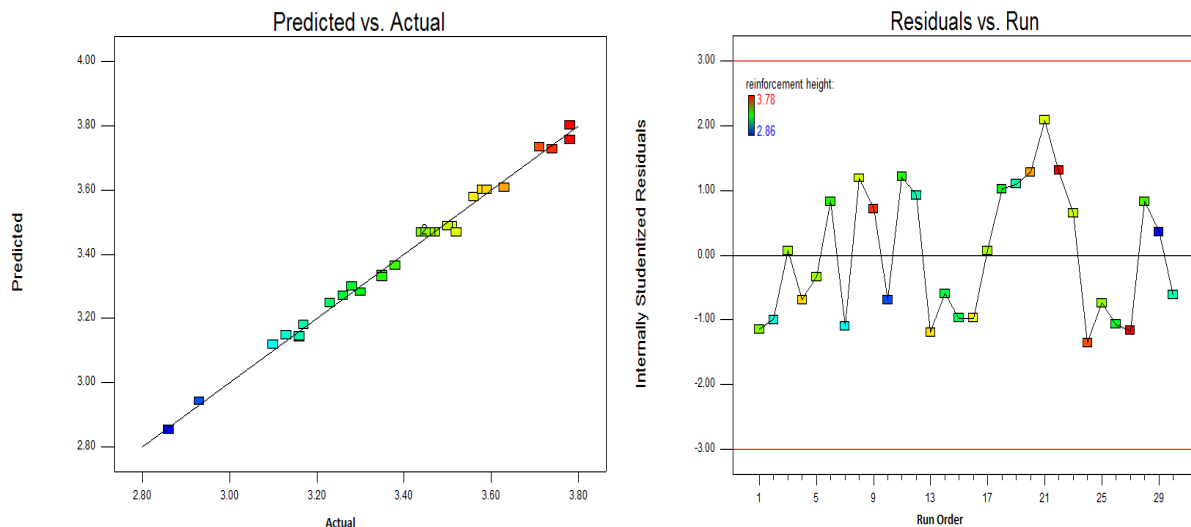


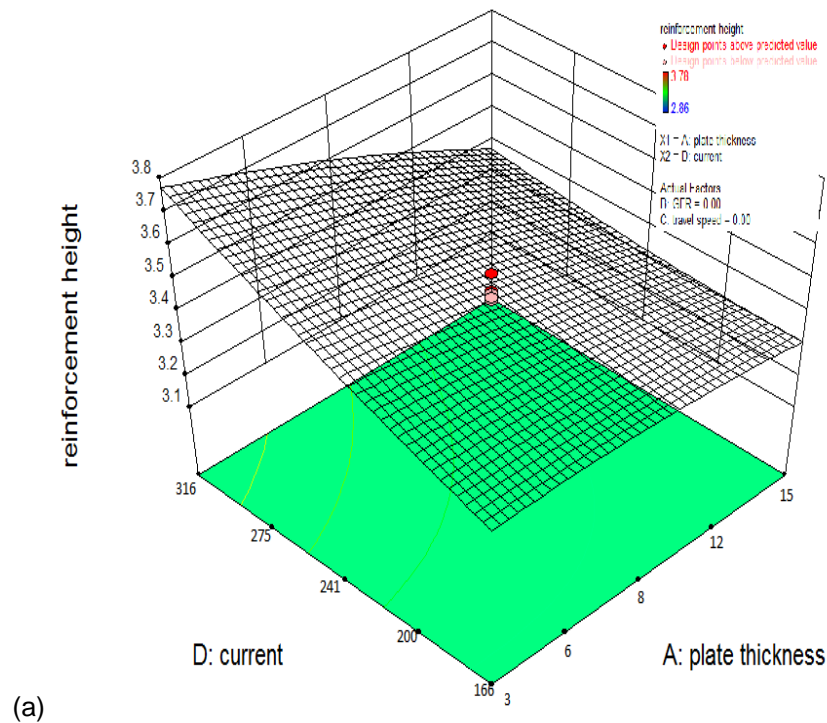
Figure 5.2(a) Predicted Vs Actual (b) Residual Vs Run

The predicted reinforcement height values are compared to their respective target values for 30 test cases is shown in figure 5.2(a). The best fit line is found to deviate a bit from the ideal $y = x$ line. Moreover, the predicted values are found to be nearby from the target values. Figure 5.2(b) shows the comparison of the residuals and run order. It shows that how to varies the residual values with run order. The lowest

residual value is observed for 24th run order and it is -1.62. The highest residual value is observed for 21st run order and it is found 2.23.

5.2.1 Interaction effect of parameters on H:

It is observed that the reinforcement height increases with increase in all values of current A. Also it can be seen that the increase in the value of the reinforcement height is most pronounced in the case of +2 level of current i.e. 316A. This is due to the fact that upon increasing the current the power per unit length of the weld bead and current density both increases, causing larger volume of base material to melt, thus increasing the reinforcement height. This trend is also supported by the positive value of co-efficient of A in the direct effect of reinforcement height.



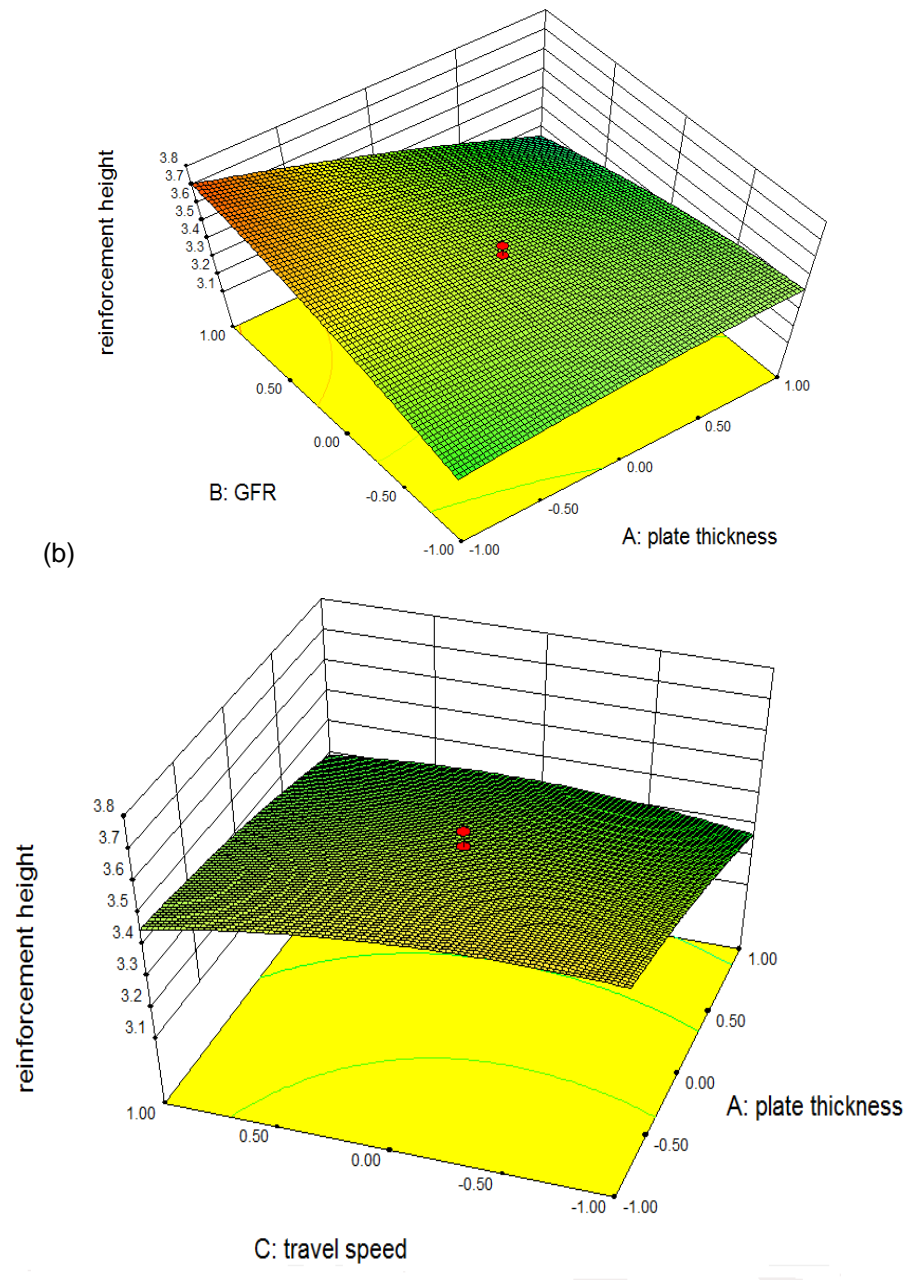


Figure 5.3 (a), (b), (c), Surface and contour plots showing interaction effect of T, S, G and I on H

It is also observed that the reinforcement height decreases with increase in travel speed for all values from -2 to 2 levels. This is because of the fact that when the welding torch travels at a greater speed over the base metal the line power per unit length of weld bead is reduced and also the welding torch covers more distance per unit time.

5.3 Effects of process parameters on bead width

The bead width varies from 6.55mm to 10.22 mm at various welding parameters i.e. plate thickness, GFR, Travel speed and current. The width increased from 7.76mm to 9.82 when current increased low level to high level. Bead width decreases steadily as the travel speed is increased.

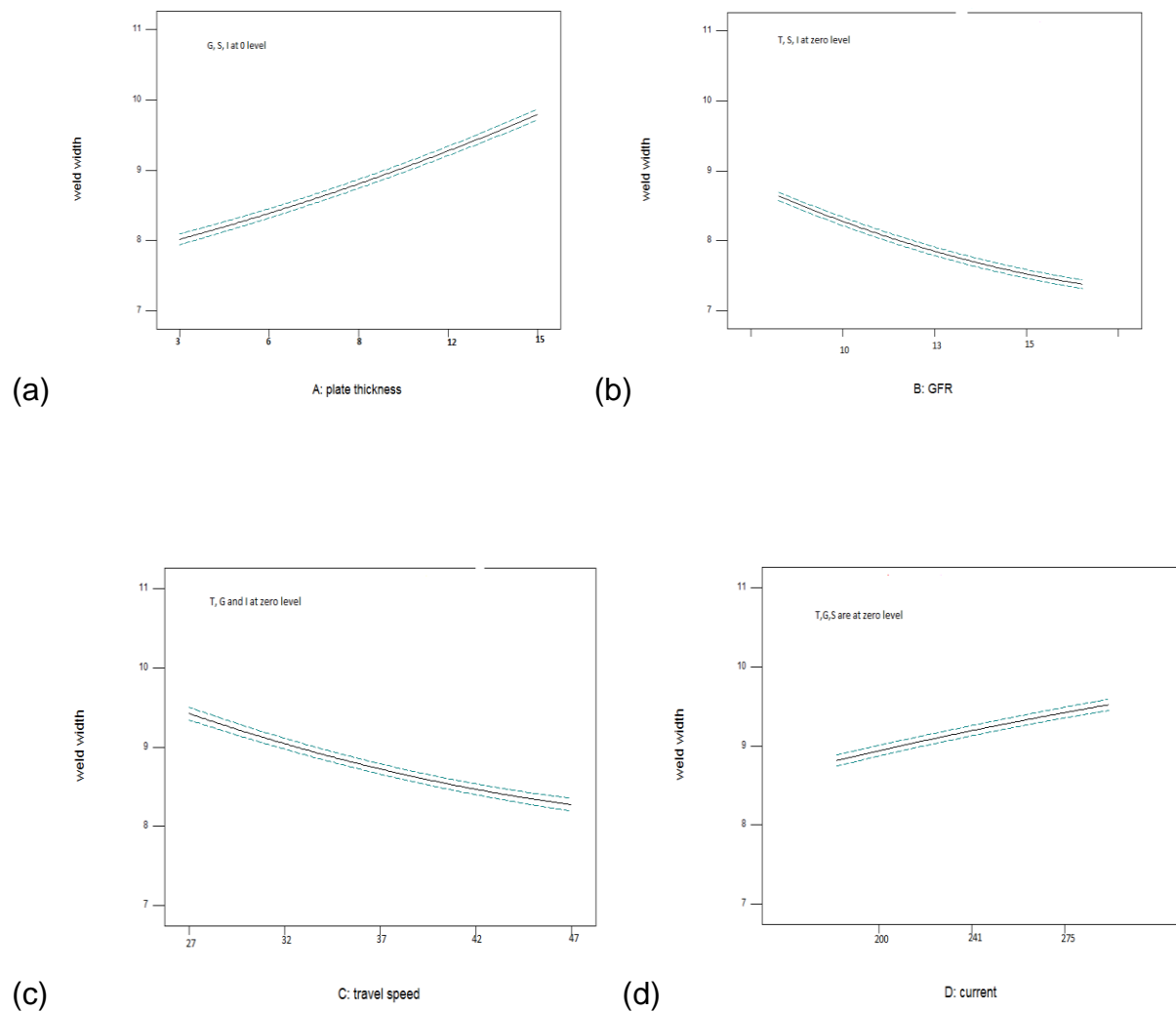


Figure 5.4 Effect of weld parameters on bead width

This is due to the fact that with increase in speed the thermal energy transmitted to the base plate from the arc or line power per unit of the weld bead decreases and less filler material is deposited per unit length of the weld bead resulting in thinner and narrower weld bead. It is safe to conclude at lower travel speeds, the weld bead is larger in mass and vice versa. As current increases, this results in more melting of work piece surface instead of melting the work piece. This ultimately results in wider bead.

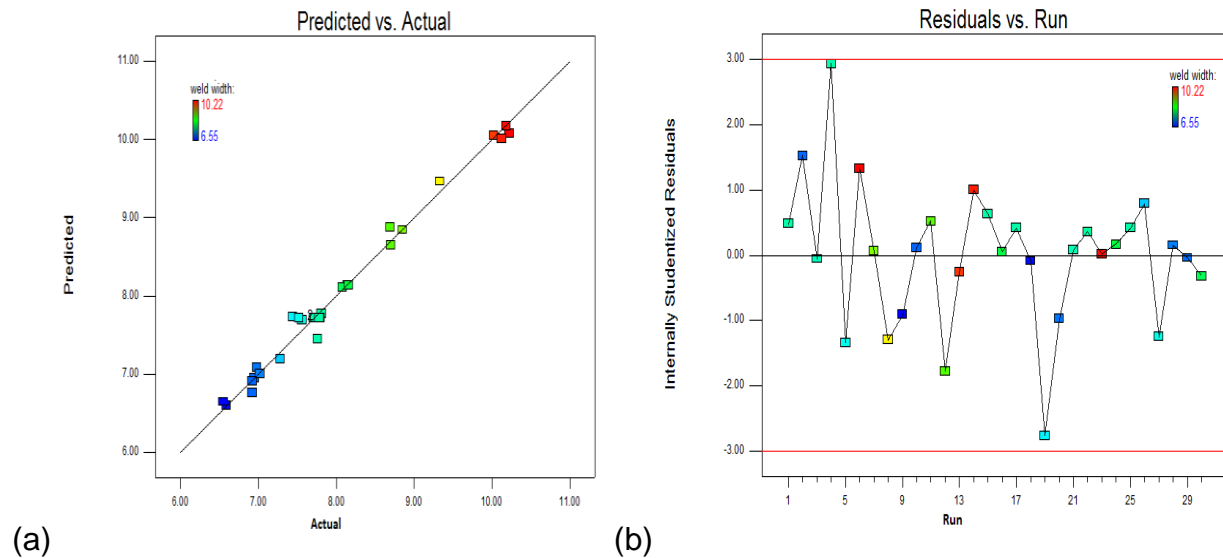
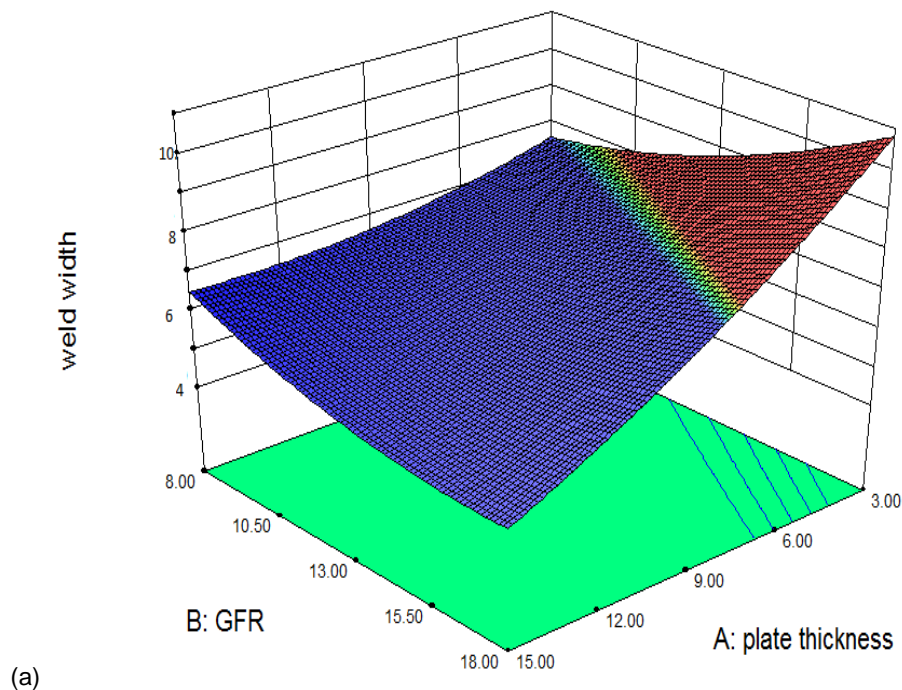


Figure 5.5(a) Predicted Vs Actual for bead width (b) Residual Vs Run for bead width

The predicted bead width values are compared to their respective target values for 30 test cases is shown in figure 5.5(a). The best fit line is found to deviate a bit from the ideal $y = x$ line. Moreover, the predicted values are found to be nearby from the target values. Figure 5.5(b) shows the comparison of the residuals and run order. It shows that how to varies the residual values with run order. The lowest residual value is observed for 19th run order and it is -2.91. The highest residual value is observed for 4th run order and it is found 2.995.

5.3.1 Interaction effect of parameters on **W**

It was observe that with increase in current, the bead width increase for all levels of current when the travel speed is decreasing. Increase in current basically results in higher melting rate of wire. Travel speed and current both have conflicting effects on the bead width. We already discussed that bead width decreases steadily as the travel speed is increased. This is due to the fact that with increase in speed the thermal energy transmitted to the base plate form the arc or line power per unit of the weld bead decreases. As plate thickness is increased the bead width is decreases. The interactions between welding parameters and bead width are shown in figure 5.6



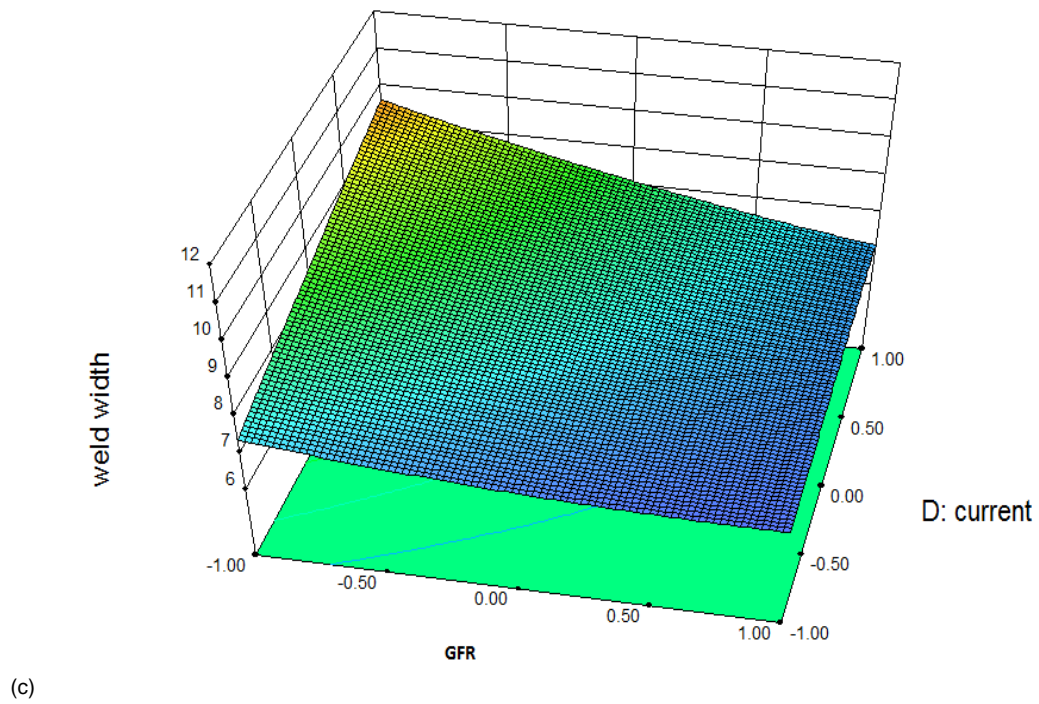
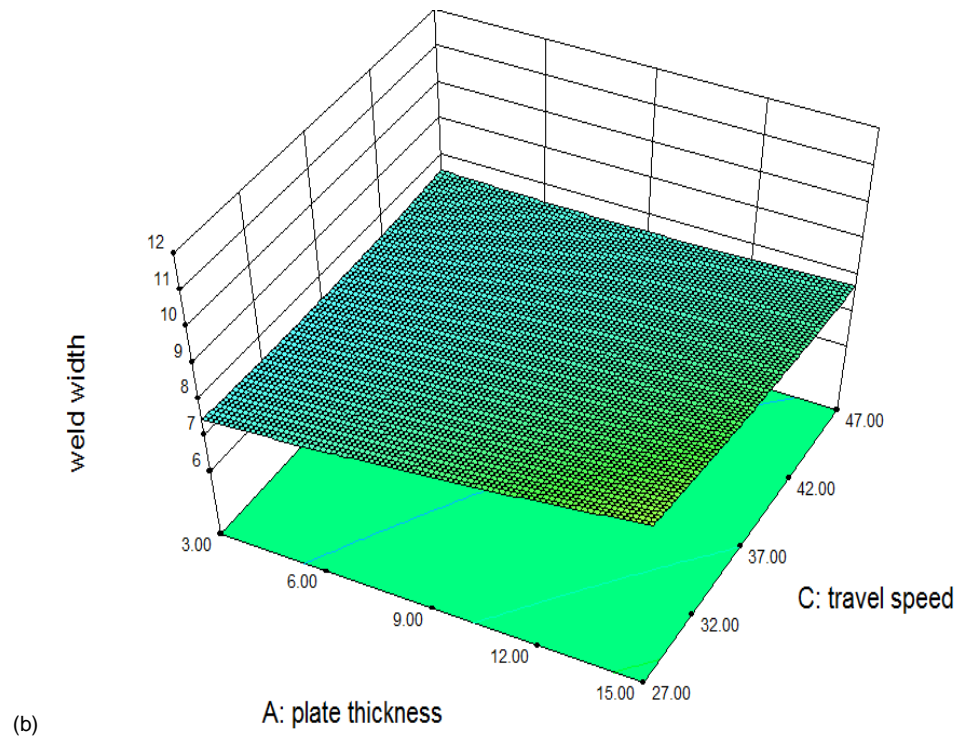


Figure 5.6 (a), (b), (c), Surface and contour plots showing interaction effect of T, S, G and I on W

5.4 Effects of process parameters on depth of penetration

It is observed that travel speed has negative effect on all the bead parameters. This is because of the fact that when the welding torch travels at a greater speed over the base metal the line power per unit length of weld bead is reduced and also the welding torch covers more distance per unit time. The combined effect of lesser line power and faster electrode travel speed results in decreased metal deposition rate per unit length of the bead. Thus the penetration decreases

For higher levels of current the rate of increase in penetration is steeper than the increase in reinforcement height. This is due to the fact that upon increasing the current the power per unit length of the weld bead and current density both increases, causing larger volume of base material to melt.

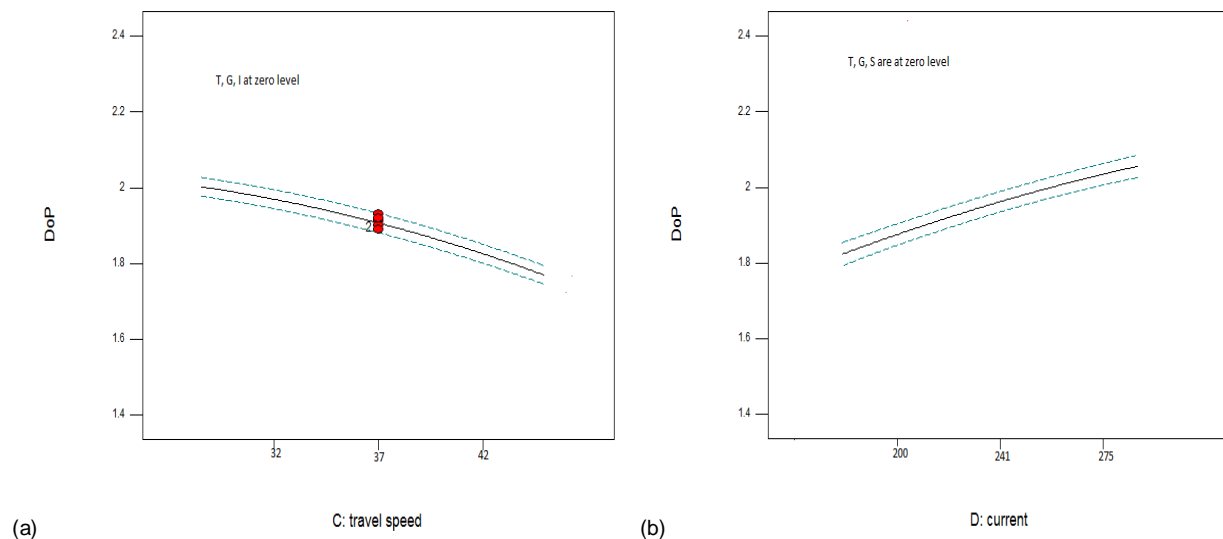


Figure 5.7 Effect of weld parameters on depth of penetration

As current increases, the temperature also increases and hence the heat content of the droplets increases which results in more heat being transferred to the base metal. Increase in current also results in increased momentum of the droplets which on striking the weld pool causes deeper penetration.

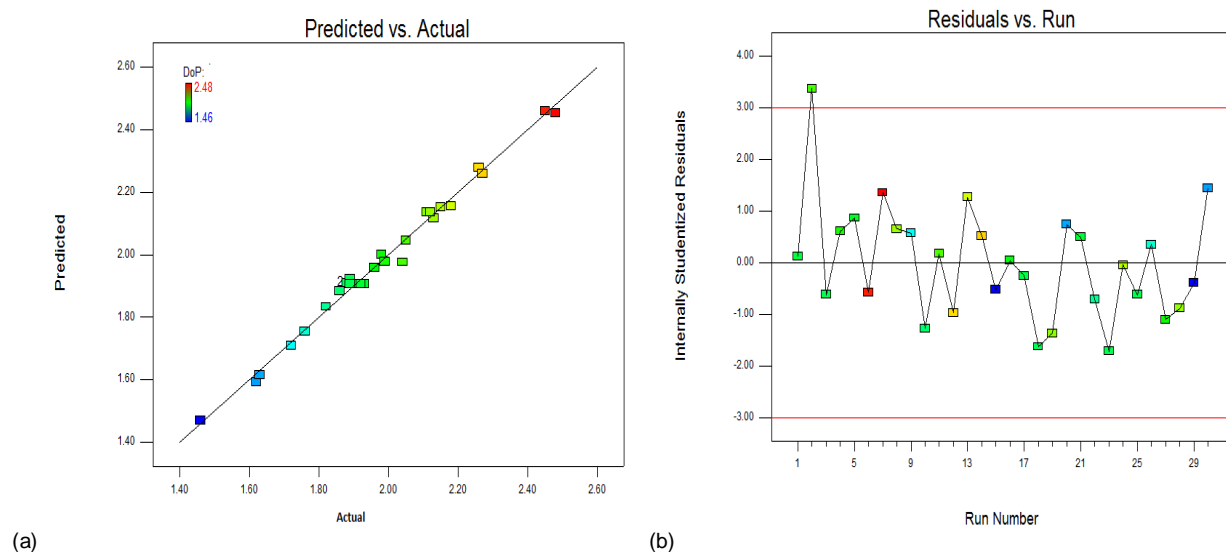
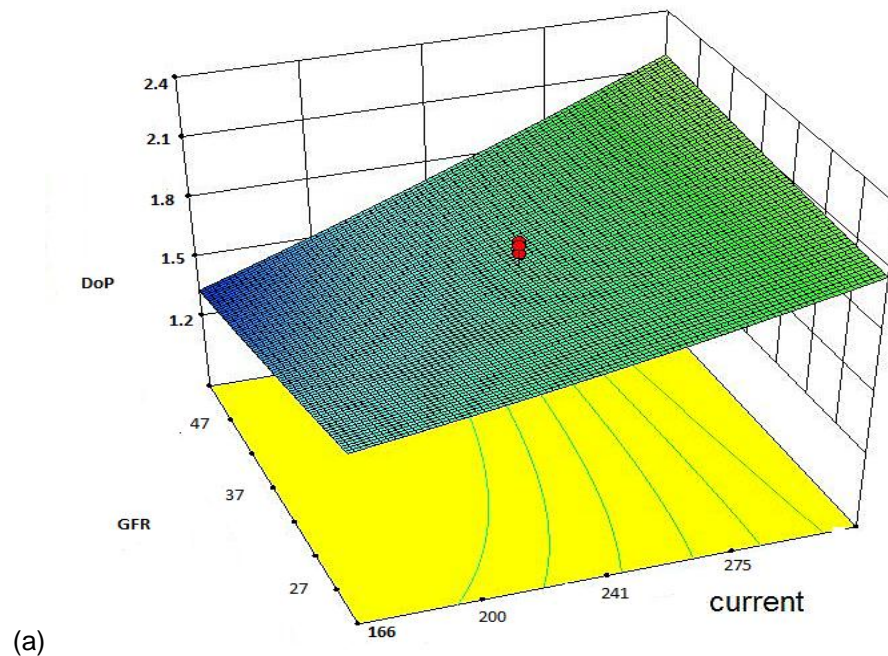


Figure 5.8(a) Predicted Vs Actual for P (b) Residual Vs Run for P

The predicted depth of penetration values are compared to their respective target values for 30 test cases is shown in figure 5.8(a). The best fit line is found to deviate a bit from the ideal $y = x$ line. Moreover, the predicted values are found to be nearby from the target values. Figure 5.5(b) shows the comparison of the residuals and run order. It shows that how to varies the residual values with run order. The lowest residual value is observed for 23rd run order and it is -1.91. The highest residual value is observed for 2nd run order and it is found 3.46.

5.4.1 Interaction effect of parameters on P

As discussed earlier; an increasing the current results in an increase of both the power per unit length of the weld bead and current density, hence causing larger volume of base material to melt. As current increases the temperature and hence the heat content of the droplets increases, which results in more heat being transferred to the base metal. Increase in current also results in increased momentum of the droplets which on striking the weld pool causes deeper penetration. As a result deeper penetration is observed. As GFR decreases, the depth of penetration increases. The figures are shown below:



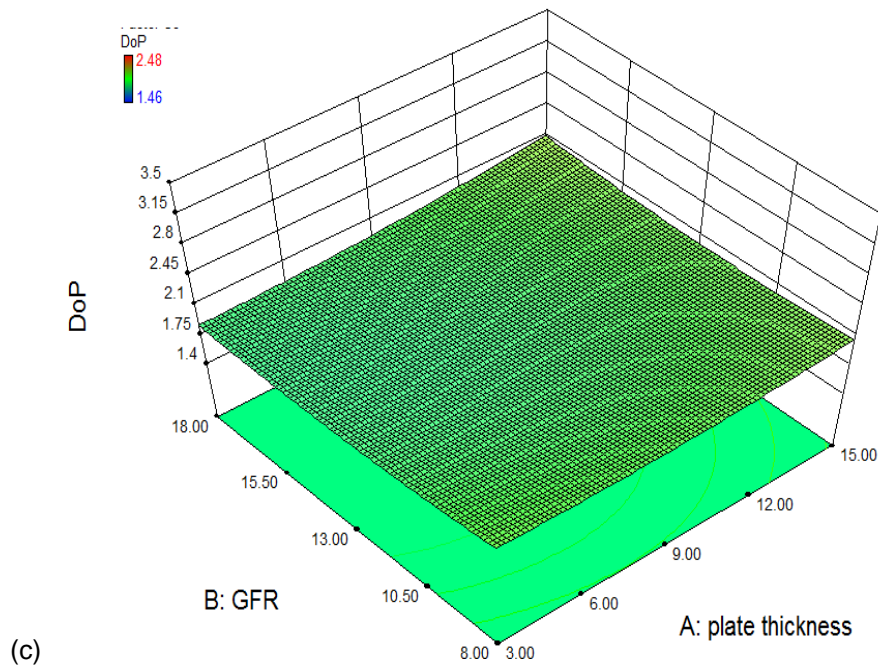
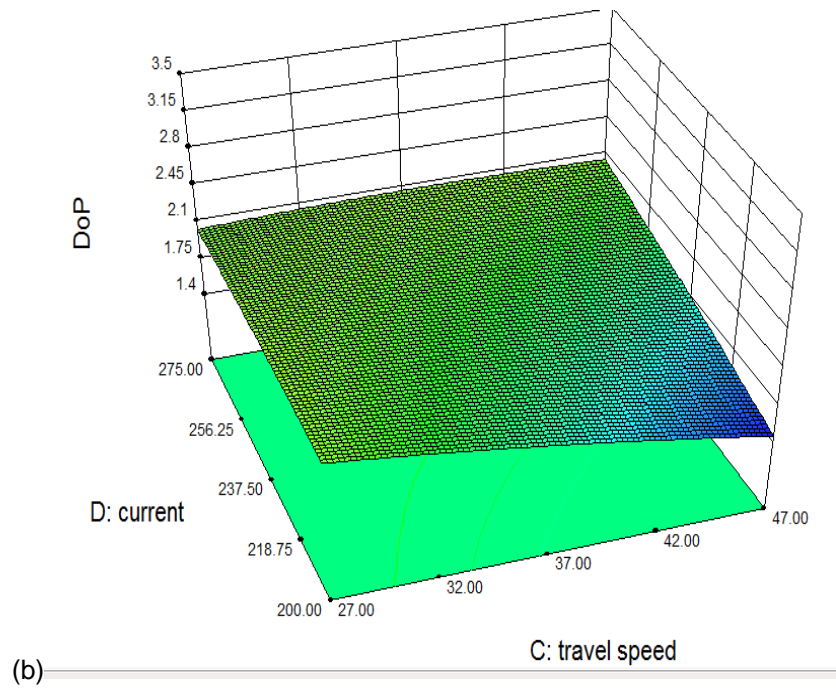


Figure 5.9 (a), (b), (c), Surface and contour plots showing interaction effect of T, S, G and I on P

The depth of penetration increases with increasing gas flow rate up to point which was the optimum value to obtain maximum penetration, because it begins to slightly decreasing after this point again linearly.

5.5 Metallurgical analysis

To carry out the metallurgical studies, specimens were cut in the transverse direction from the welded plates. After that, the specimens were polished with progressively finer grades of emery paper. After that wet polishing of the specimen was done; followed by etching with ferric chloride and hydrochloric acid etching reagent. Its composition is ferric chloride (5g), hydrochloric acid (50ml), and water (10ml). Microstructural studies were carried out on the weld zone, Heat Affected Zone and the Base metal, after preparing the specimens. Studies were carried out for the sample with maximum heat input and the sample with minimum heat input. The variation of micro hardness along the weld bead in horizontal direction was also determined.

5.5.1 Microstructural Analysis

Microstructure is defined as the structure of a prepared surface or thin foil of material as revealed by a microscope above 25× magnification. The microstructure of a material can strongly influence physical properties such as strength, toughness, ductility, hardness, corrosion resistance, high/low temperature behaviour, wear resistance, and so on, which in turn govern the application of these materials in industrial practice. The microstructural features of a given material may vary greatly when observed at different length scales. For this reason, it is crucial to consider the length scale of the observations when describing the microstructure of a material. To study the

microstructure Olympus GX 41 microscope was used in conjunction with META-Lite software.



Figure 5.10 Olympus GX 41 microscope

From the design matrix we see that the current is high and the travel speed is low for trial number 9, 10, 11 and 12. Thus these trials represent the maximum Heat input. In the microstructural analysis the different phases present in the microstructure. Figure 5.10 presents exemplary structure of above samples as delivered.

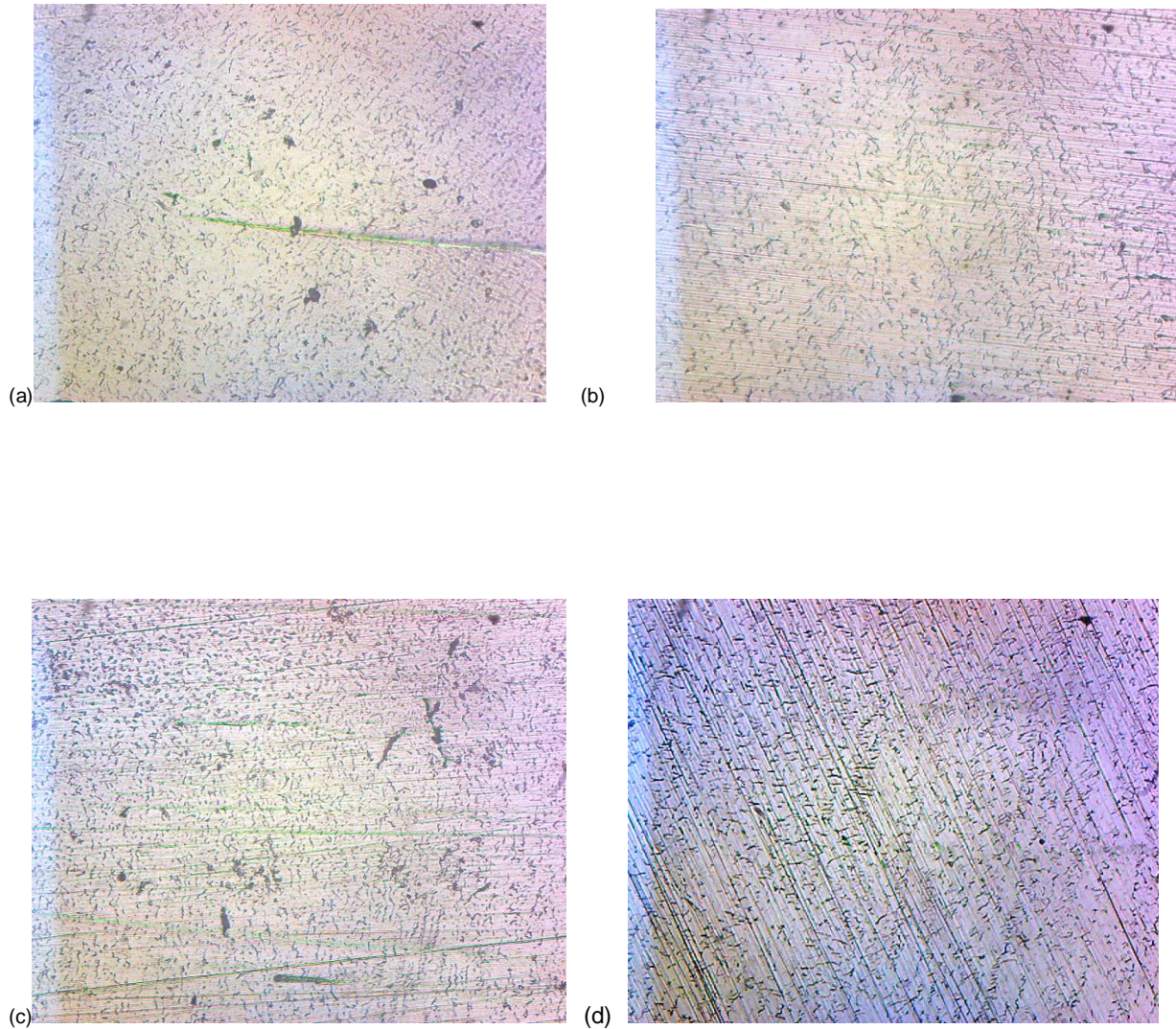


Fig 5.11 Micro structure (200 μm) at high heat input: (a) run order 09, (b) run order 10, (c) run order 11, (d) run order 12

The microstructure is shown above. In the micro structure the inclusions and porosity were found. These inclusions and porosity may be due to carbon dioxide in the shielding gas composition. The size of pores and inclusions are small as current increases. From the design matrix we see that the current is high and the travel speed is low for trial number 1, 5, 7 and 8. Thus these trials represent the minimum Heat input. In the microstructural analysis the different phases present in the microstructure. Figure

5.12 presents exemplary structure of above samples as delivered. In the micro structure of these it was observed that inclusions are more and the sizes of pores are large. In the Heat affected zones martensite or bainite structures using optical metallography were not found.

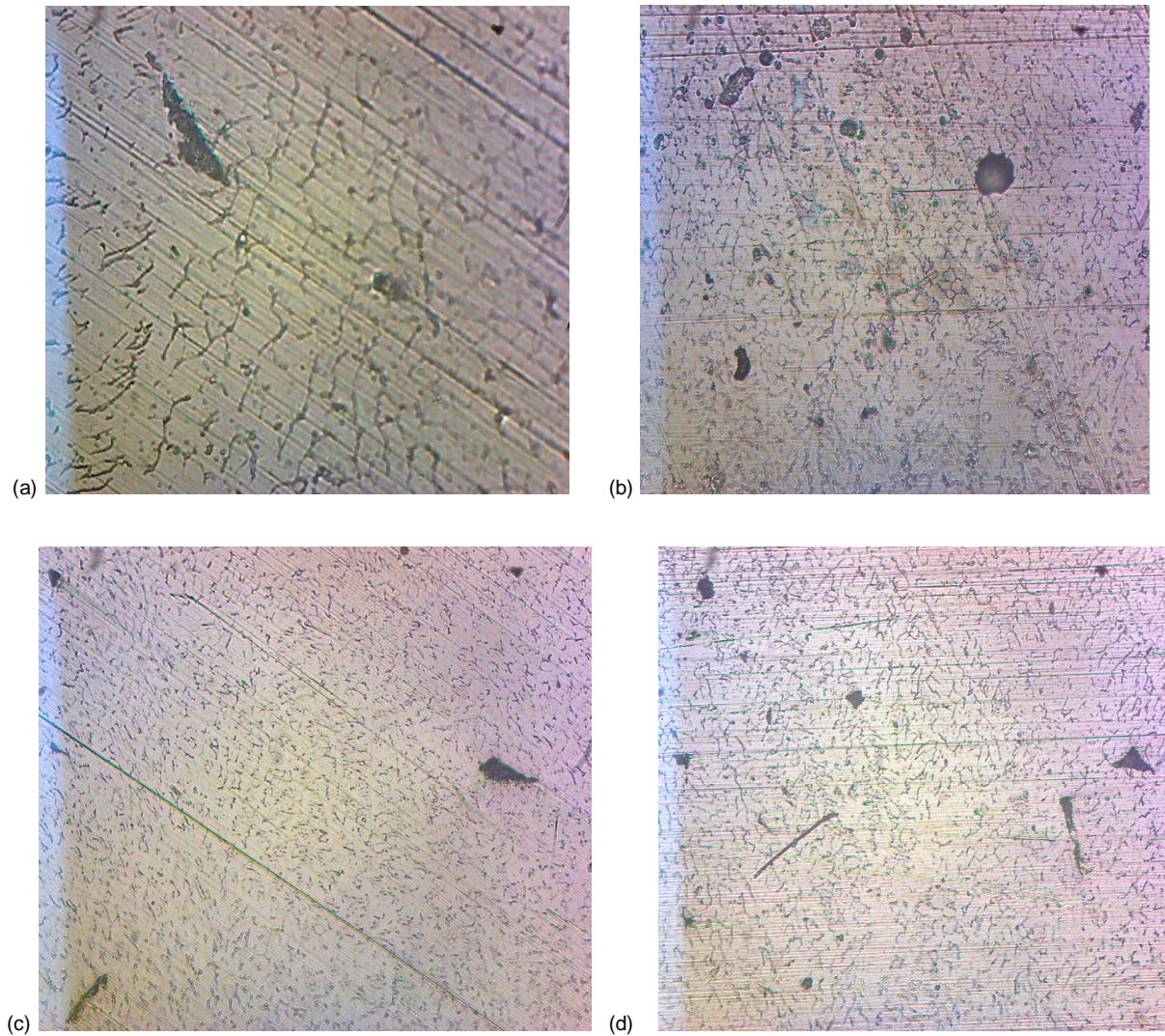


Fig 5.12 Micro structure at low heat input: (a) run order 1 at 500 μm , (b) run order 5 at 200 μm , (c) run order 7 at 200 μm , (d) run order 8 at 200 μm

5.5.2 Micro hardness

Variation of micro hardness was observed at the various points. To measure the micro hardness, Omnitech MVH Auto Micro Hardness tester (Figure 5.12) was used with 100 gram load and dwell time of 20 seconds.



Figure 5.13 Omnitech MVH Auto Micro Hardness tester

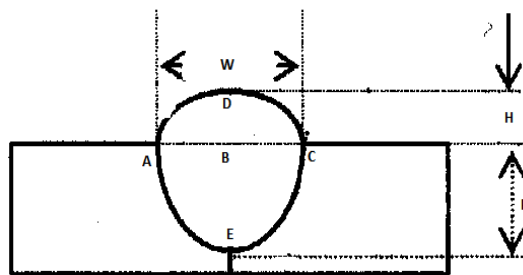


Figure 5.14 Varies points on bead to measure the micro hardness

The micro hardness values were calculated at various points. These points are at different -2 regions, starting from point A to point E. The points are shown in figure 5.13. The values reported are for Knoop's Micro hardness. A pyramidal diamond point is pressed into the polished surface of the test material with a known force, for a specified dwell time, and the resulting indentation is measured using a microscope.

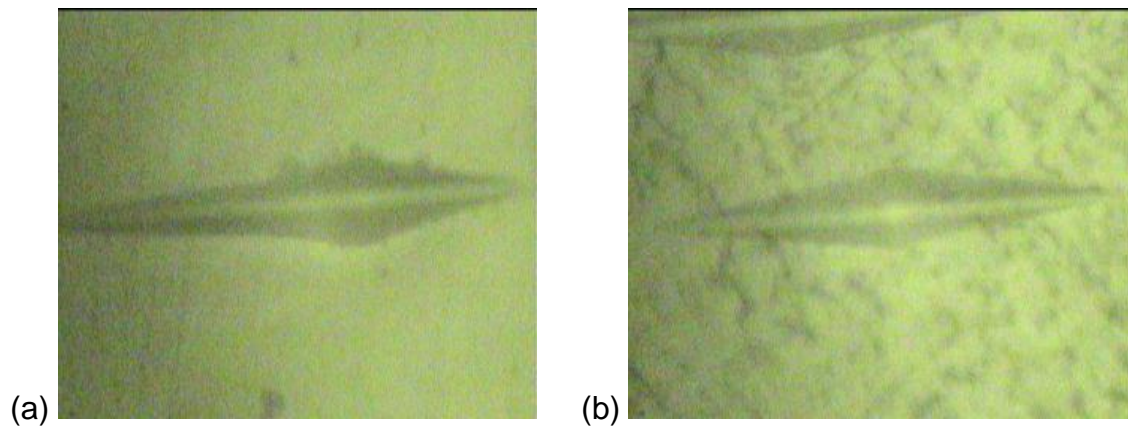


Figure 5.15 micro indentation

The geometry of this indenter is an extended pyramid with the length to width ratio being 7:1. The depth of the indentation can be approximated as $1/30$ of the long dimension. The calculated values of micro hardness are shown in table 5.1

Sample no.	A	B	C	D	E
1	1361	1274	1381	1268	1394
2	1275	1252	1285	1226	1298
3	1281	1220	1285	1151	1509
4	1428	1402	1426	1348	1488
5	1701	1565	1712	1601	1695

6	1367	1321	1382	1288	1370
7	1465	1532	1365	1446	1506
8	1312	1296	1310	1245	1420
9	1613	1714	1601	1436	1802
10	1477	1456	1482	1330	1601
11	1499	1477	1525	1261	1467
12	1589	1505	1598	1498	1605
13	1298	1261	1302	1236	1312
14	1375	1330	1363	1284	1375
15	1625	1543	1662	1436	1640
16	1406	1505	1455	1512	1395
17	1750	1662	1705	1455	1782
18	1254	1258	1243	1228	1301
19	1367	1278	1398	1261	1312
20	1625	1520	1675	1605	1807
21	1688	1339	1580	1245	1360
22	1261	1302	1236	1312	1298
23	1543	1470	1565	1442	1525
24	1578	1442	1589	1412	1552
25	1385	1312	1402	1289	1439
26	1765	1702	1755	1625	1768
27	1348	1467	1301	1261	1675
28	1499	1662	1312	1369	1386
29	1289	1265	1306	1245	1365
30	1446	1520	1502	1212	1426

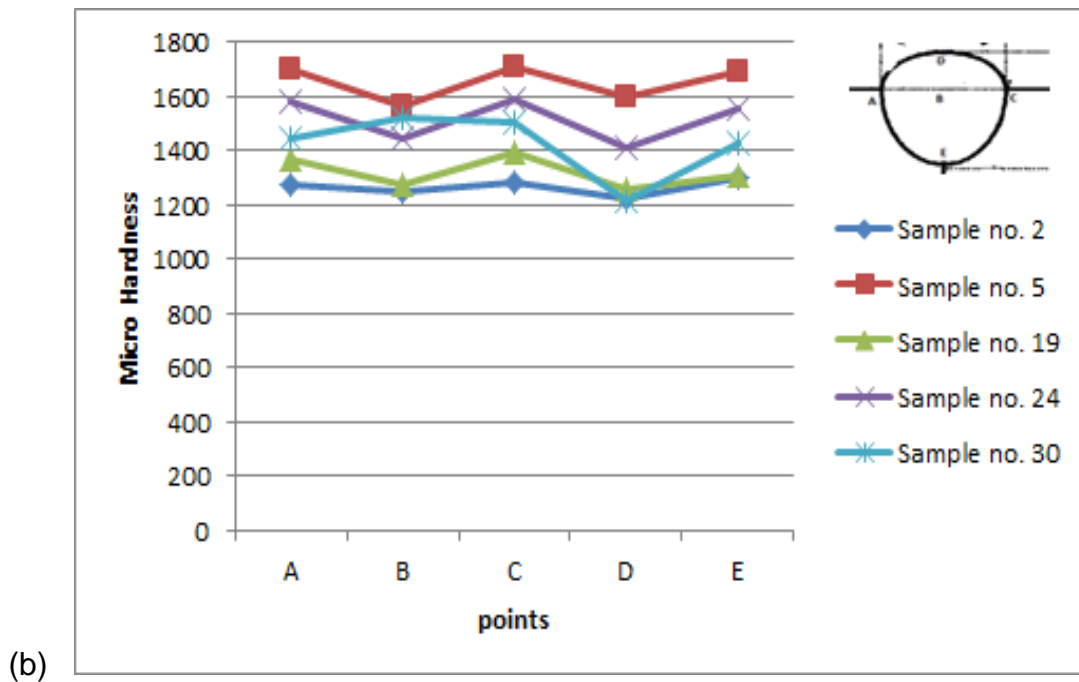
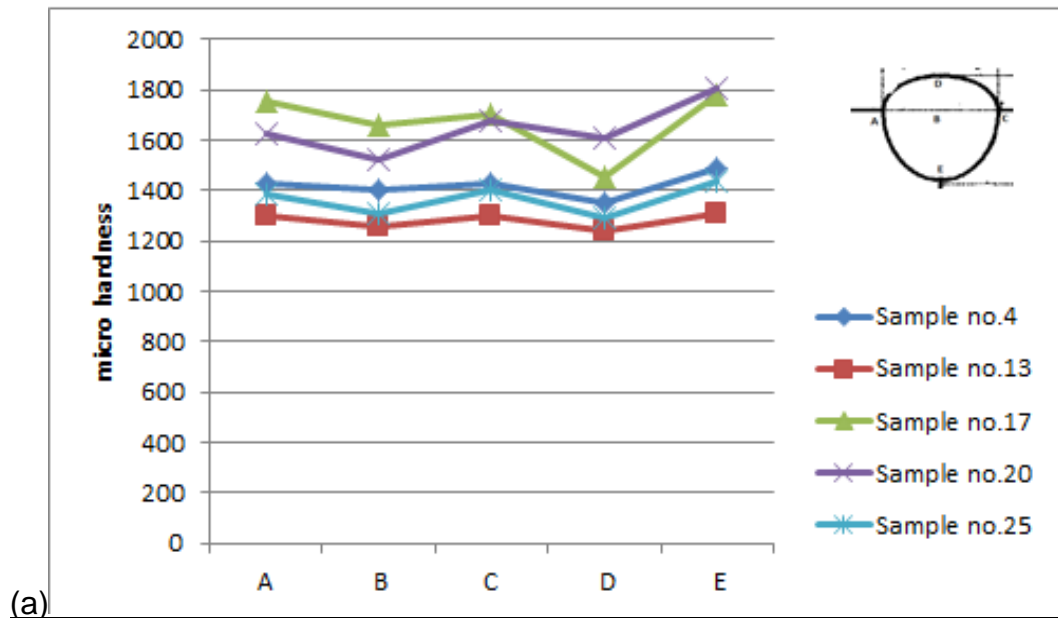


Figure5.16: Variation of micro hardness at different regions

The micro hardness values at different point are obtained. For base metal the micro hardness value is measured as 1125KHN. The graphs are plotted between micro hardness and various points. The hardness measurements were carried out at a depth of 2 mm from the base metal surface. From above table we see that the KHN value for the weld zone and the base metal are comparable while maximum hardness is observed at point A, C and E. These points are in the heat affected zone (HAZ). So the maximum micro hardness value is observed in in HAZ. This observation can be attributed to pearlite content and the size range of the micro structure. The pearlite content and the range of size distribution for the base metal and the weld zone are almost same. While the pearlite content for the HAZ is higher and greater numbers of grains are in the lower range, indicating finer microstructure; as compared to weld zone and base metal. The increased pearlite content combined with finer microstructure results in greater micro hardness in the HAZ. Also it can be observed that the micro hardness is greatest in the grain refined region, having the highest Pearlite content and where the grains are finest

CHAPTER 6

CONCLUSIONS AND FUTURE SCOPE

6.1 Conclusion

From the results, the conclusions were drawn:

1. With the use of oscilloscope, it is possible to observe the format of the current and voltage produced by welding processes. These signal waves may mimic some metal transfer modes. For instance, during short-circuiting transfer, when the droplet is starting its development, voltage oscillates around a mean value but tends to zero when the drop touches the pool (short circuit).
2. High welding current and high welding voltage produced the mixed mode but predominantly axial spray and occasional short circuiting transfer between. The weld bead ripple were fairly uniform and the general appearances of the bead were very good.
3. The mathematical models developed can be used for successful prediction of bead geometry features within the pre decided range of the parameters.
4. The mathematical models show fair degree of accuracy in predicting the bead geometry features
5. It was observed that the welding current has positive effect on all the bead geometry parameters while welding speed has negative effect on the bead parameters.

6. All the relationships are linear in nature and can be effectively utilized for optimizing the conditions for a specific bead dimension.
7. Microstructure of the weld metal resulting that size of pores is smaller when current is increased from low level to high level and inclusions are more when current decreases.
8. Micro hardness value is maximum in HAZ. This results that the grain sizes are finest in the HAZ. The micro hardness value increases from base metal to HAZ

6.2 Future Scope

- In this study, selected parameters are plate thickness, GFR, Travel speed and current. Study can be done by selecting more parameters such as voltage, nozzle-to-plate distance, electrode angle and shielding gas mixture.
- Apart from the micro hardness and metallurgy, studies can be undertaken to analyse the effect of process parameters on the mechanical properties of the joint, like Toughness, Ultimate Tensile Strength etc.
- Scanning electrode microscopy and X-ray Diffraction can be done for various welding parameters.

REFERENCES

1. E. Karadeniz, Ozsarac, U. and Yildiz, C. 2007. "The effect of process parameters on penetration in gas metal arc welding process", Materials and Design. Vol 28 , Issue 2 , pp. 649-656.
2. M. Suban and J. Tusek, 2003. "Methods for the determination of arc stability", Journal of Materials Processing Technology, pp. 430-437
3. Jonsson J, Murphy PG, Zeckely AB. 1995 "Influence of oxygen additions on argonshielded gas metal arc welding processes". Weld J;74(2):48s–58s.
4. Kim I.S., Basu A.and Siores E., 1996 "Mathematical models for control of weld bead penetration in GMAW process". International journal of advanced manufacturing technology, vol 12, pp 393-401.
5. Kim I.S., Son K.J, Yang Y.S. and Yaragada P.K.D.V., 2003 "sensitivity analysis for process parameters in GMAW process using a factorial design method". International journal of machine tools and manufacture, vol 43,pp736-769
6. Ganjigatti J.P., Pratihari D.K. Roychoudhury A. 2008 "modeling of MIG welding process using statistical approaches,". International journal of advanced manufacturing technology, vol 35 pp 1166-1190
7. Ganjigatti J.P., Pratihari D.K. Roychoudhury A. 2007 "Global versus cluster-wise regression analysis for prediction of bead geometry in MIG welding process". Journal of materials processing technology, vol 189, pp 352-366
8. Karadeniz E , Ozsarac U, Yildiz C, 2007, "The effect of process parameters on penetration in gas metal arc welding processes" Materials and Design; 28: 649–656
9. Pires RM, Quintino I and Miranda L. 2006 "Analysis of the influence of shielding gas mixtures on the gas metal arc welding metal transfer modes and fume formation rate". Material and Design J;28(5):1623–31.

10. Palani P.K. and Murugun N., 2006 "Development of mathematical models for prediction of weld bead geometry in cladding by flux cored arc welding". International journal of advanced technology, vol 30, pp 669-679.
11. Manoj Singla, Dharminder Singh and Dharmpal Deepak. 2010 "Parametric Optimization of Gas Metal Arc Welding Processes by Using Factorial Design Approach". Journal of Minerals & Materials Characterization & Engineering, Vol. 9, No.4, pp.353-363,
12. Gunaraj V, Murugan N, 1999, "Application of response surface methodology for predicting weld bead quality in submerged arc welding of pipes". Journal of Material Processing Technology; 88:266–275.
13. Gunaraj V, Murugan N, 1999, "Prediction and comparison of the area of the heat-affected zone for the bead-on-plates and bead-on-joint in submerged arc welding of pipes" Journal of Material Processing and Technology; 95: 246–261.
14. Murugan N., Parmar R.S and Sud S.K, 1999, "Effect of submerged arc process variables on dilution and bead geometry in single wire surfacing". Journal of Material Processing and Technology, vol 371, pp 767-780
15. Murugan N. and Parmar R.S., 1994, "Effect of MIG process parameters on the geometry of the bead in the automatic surfacing of stainless steel". Journal of Material Processing and Technology, vol 41, pp 381-398
16. Shahi A.S. and Pandey Sunil, 2008 "Modeling of the effects of welding conditions on dilution of stainless steel cladding produced by GMAW procedures". International journal of advanced technology, vol.30, pp 669-676
17. Muruganan N, Gunaraj V, 2005, "Prediction and control of weld bead geometry and shape relationships in submerged arc welding of pipes" Journal of Materials Processing Technology; 168 : 478–487
18. Koleva E. 2005, "Electron beam weld parameters and thermal efficiency improvement" Vacuum J ; 77 : 413–421

19. Eroglu M , Aksoy M , Orhan N, 1999, "Effect of coarse initial grain size on microstructure and mechanical properties of weld metal and HAZ of a low carbon steel" *Material Science and Engineering*; A269: 59-66
20. Kiran D.V, Basu B, De A, 2012, "Influence of process variables on weld bead quality in two wire tandem submerged arc welding of HSLA steel" *Journal of Material Processing Technology*, doi:10.1016/j.jmatprotec.2012.05.008
21. Gunaraj V, Murugan N, 1999, "Prediction and comparison of the area of the heat-affected zone for the bead-on-plate and bead-on-joint in submerged arc welding of pipes" , *Journal of Material Processing Technology*; 95 : 246-261
22. Kolhe K.P, Datta C.K , 2008, "Prediction of microstructure and mechanical properties of multipass SAW" *Journal of Material Processing Technology*; 197: 241-249
23. Shanping LU, Hidetoshi L and Kiyoshi F. 2005 "Effects of CO₂ shielding gas additions and welding speed on GTA weld shape". *J Material Science*; 40: 2481–5.
24. Kacar R and Kokemli K. 2005 "Effect of controlled atmosphere on the MIG arc weldment properties". *Material Design J*; 26(6): 508–16.
25. Subramaniam DR and White S. 2001 "Effect of shield gas composition on surface tension of steel droplets in a gas-metal-arc welding arc". *Metal Material Trans B*; 32B(2): 313–8.
26. Praveen, P.K.D.V. Yarlagadda and M.J. Kang, 2005, "Advancements in pulse gas metal arc welding", *Journal of Materials Processing Technology*, Vol. 164-165, pp. 1113- 1119.
27. P. Praveen and P.K.D.V. Yarlagadda, 2005, "Meeting challenges in welding of aluminum alloys through pulse gas metal arc welding", *Journal of Materials Processing Technology*, pp. 1106-1112.
28. Y. S. Kim, 1989, "Metal transfer in gas metal arc welding", PhD Thesis, MIT: USA.
29. J. H. Waszink and M. J. Piena, 1986 , "Experimental investigation of drop detachment and drop velocity in GMAW", *Welding Journal* , Vol. 65 , pp. 289–98
30. Randhawa, H.S. Ghosh and P.K. Gupta. 2000, "Some basic aspects of geometrical characteristics of pulsed current vertical-up GMA weld". *ISIJ Int.* 40 (1), 71–76.

31. Subramaniam, S., White, D.R., Jones, J.E. and Lyons, D.W. 1999 "Experimental approach to selection of pulsing parameters in pulsed GMAW. Weld". J. 78 (5), 166s–172s
32. Wang, G., Huang, P.G. and Zhang, Y.M. 2004 "Numerical analysis of metal transfer in gas metal arc welding under modified pulsed current conditions". Met. Mater. Trans. 35B, 857–866.
33. Ghosh, P.K., Randhawa, H.S. and Gupta, S.R. 2000 "Characteristics of a pulsed-current, vertical-up gas metal arc weld in steel". Met. Trans. 31A (12), 2247–2259.
34. Ghosh, P.K., Gupta and S.R., Randhawa. 2000. "Analytical studies on characteristics of vertical-up bead on plate weld deposition using pulsed current GMAW". International J. Join. Materials. 12 (3), 76–85.
35. McGrath, J.T., et al., 1988. "Microstructural mechanical property relationships in thick section narrow groove welds". Welding Journal. ;67: 196-s-201-s.
36. Wu, C.S., Chen, M.A., and Lu Y.F. 2005. "Effect of current waveforms on metal transfer in pulsed gas metal arc welding". Meas. Sci. Technol. 16, 2459–2465.
37. Giachino, J., Weeks, W., and Johnson, G. 1968, "Welding Technology". Chicago: American Technical Society.
38. A designers' handbook series no 9002, welding of stainless steels and other joining methods: produced by American iron and steel institute
39. Richard D. Campbell, 2004 "Avoiding Defects in Stainless Steel Welds",
40. Welder.s Handbook, 1999 Designed and produced by: PDF Conceptual Design & Marketing, Published by: Air Products PLC,
41. Pierre-Jean Cunat. 2005 "The Welding of Stainless Steels" The European stainless steel development association, Materials and Applications Series, Volume 3,
42. H. Hänninen, and J. Romu, 2001 "Trends in forming and welding of stainless steels", Helsinki university of technology, finland,

APPENDIX

Table 3.9 observation 6

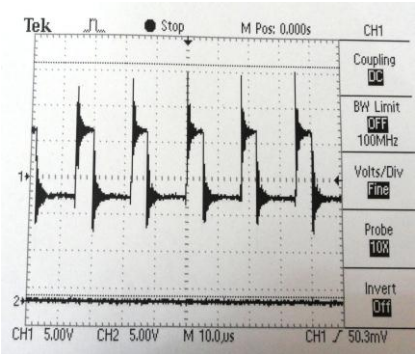

V		T	G	I	S	V	Weld bead	
		12	10	200	42	16.8		
		H		W		P		
		3.17		8.08		1.62		

Table 3.10

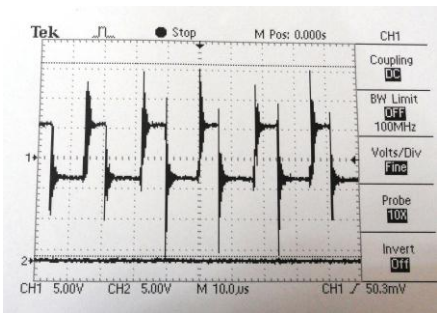

V		T	G	I	S	V	Weld bead	
		6	15	200	42	20.8		
		H		W		P		
		3.63		6.98		1.63		

Table 3.11

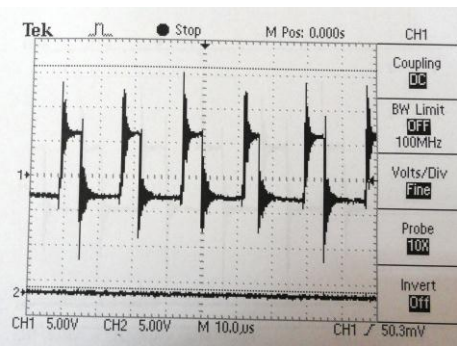

V		T	G	I	S	V	Weld bead	
		12	15	200	42	17.1		
		H		W		P		
		3.3		6.59		1.63		

Table 3.12

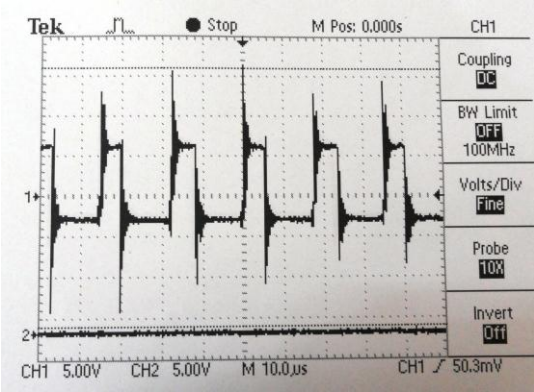

V		T	G	I	S	V	Weld bead
		6	10	275	32	25.9	
		H		W		P	
		3.71		8.16		2.15	

Table 3.13

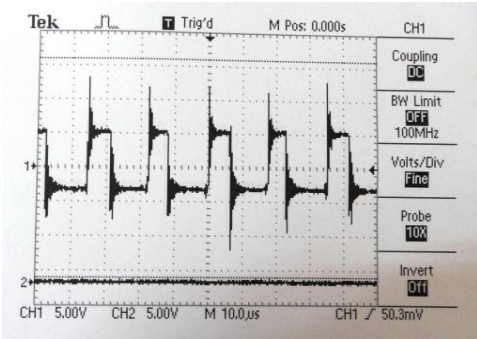

V		T	G	I	S	V	Weld bead
		8	10	275	32	21.7	
		H		W		P	
		3.58		10.02		2.18	

Table 3.14

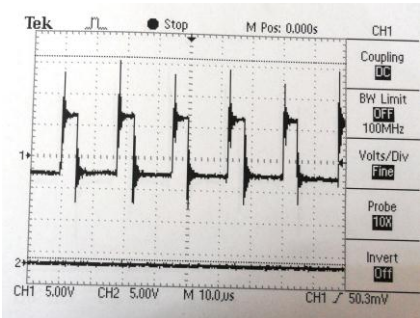

V		T	G	I	S	V	Weld bead
		6	15	275	32	25.9	
		H		W		P	
		3.74		6.55		1.72	

Table 3.15

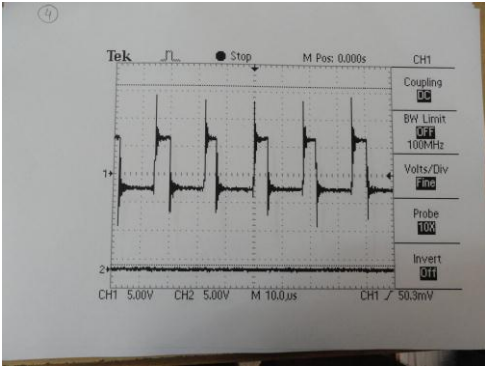

V		T	G	I	S	V	Weld bead
		12	15	275	32	22.2	
		H		W		P	
		2.93		6.92		1.86	

Table 3.16

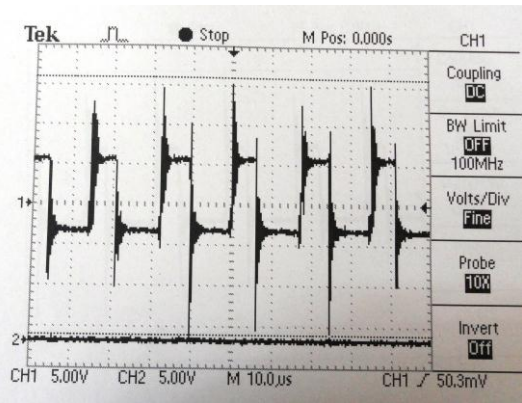

V		T	G	I	S	V	Weld bead
		6	10	241	42	25.9	
		H		W		P	
		3.51		9.33		2.13	

Table 3.17

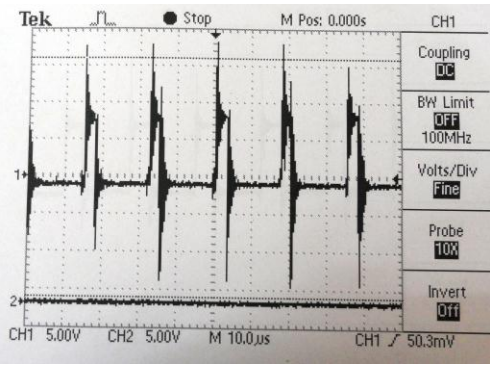

V		T	G	I	S	V	Weld bead
		12	10	275	42	21.9	
		H		W		P	
		3.5		9.33		1.89	

Table 3.18

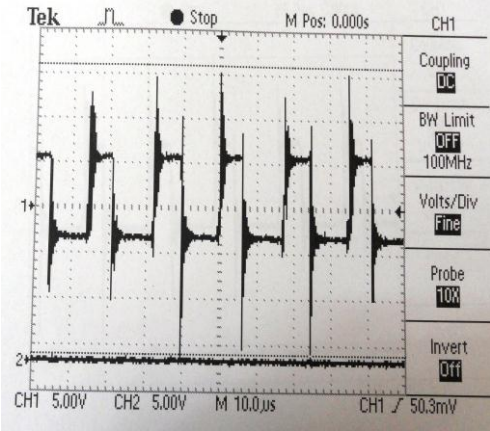

V		T	G	I	S	V	Weld bead
		6	15	275	42	25.5	
		H		W		P	
		3.78		7.56		1.98	

Table 3.19

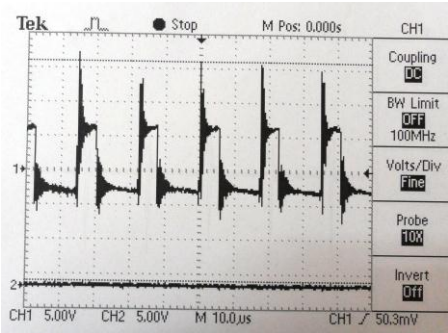

V		T	G	I	S	V	Weld bead
		12	15	275	42	21.7	
		H		W		P	
		3.13		6.92		2.04	

Table 3.20

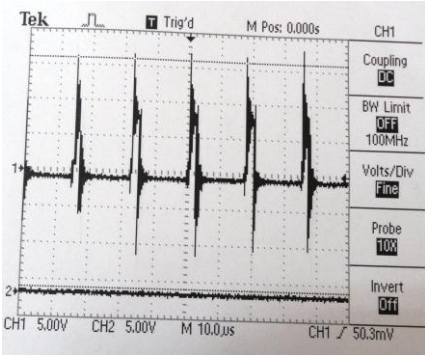

V		T	G	I	S	V	Weld bead
		3	13	241	37	27.4	
		H		W		P	
		3.59		7.76		2.04	

Table 3.21

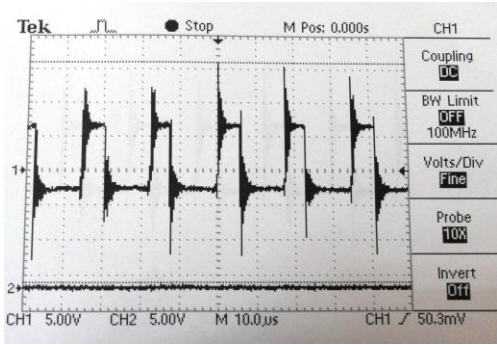

V		T	G	I	S	V	Weld bead
		15	13	241	37	23.5	
		H		W		P	
		3.16		8.6		2.26	

Table 3.23

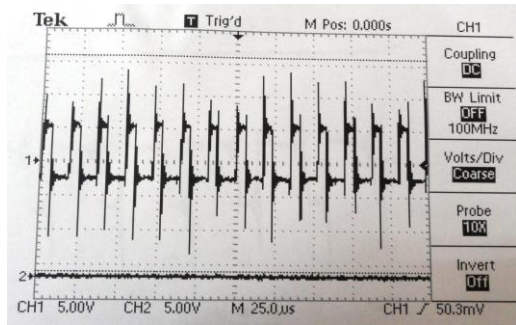

V		T	G	I	S	V	Weld bead
		8	8	241	37	24.1	
		H		W		P	
		3.26		10.12		2.27	

Table 3.24

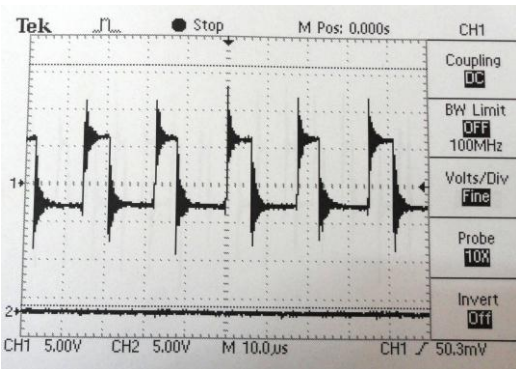

V		T	G	I	S	V	Weld bead
		8	18	241	37	23.7	
		H		W		P	
		3.38		7.02		2.12	

Table 3.25

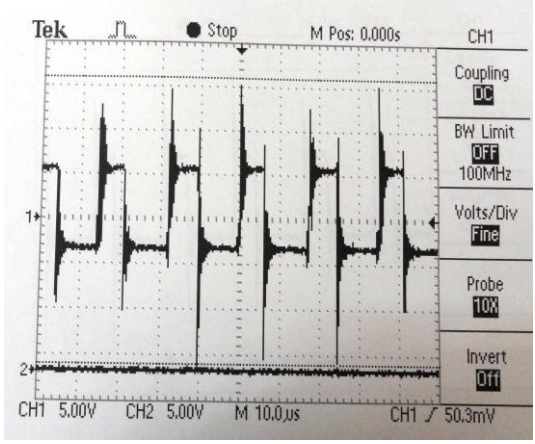

V		T	G	I	S	V	Weld bead
		8	13	241	27	23.8	
		H		W		P	
		3.35		8.7		1.9	

Table 3.26

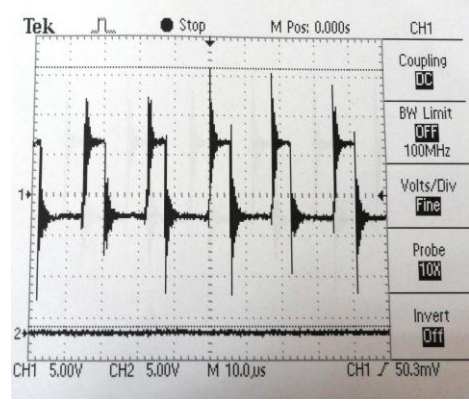

V		T	G	I	S	V	Weld bead
		8	13	241	47	23.8	
		H		W		P	
		3.23		7.79		1.9	

Table 3.27

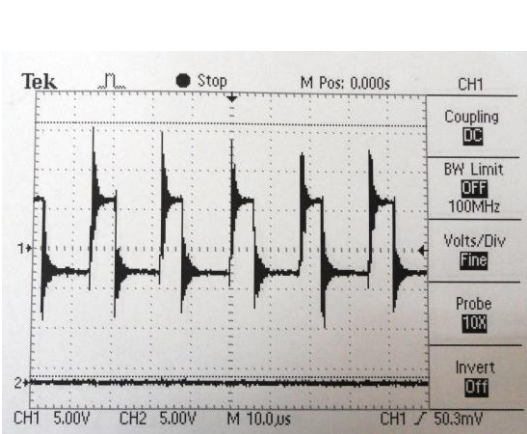

V		T	G	I	S	V	Weld bead
		8	13	166	37	27.3	
		H		W		P	
		3.28		7.28		1.76	

Table 3.28

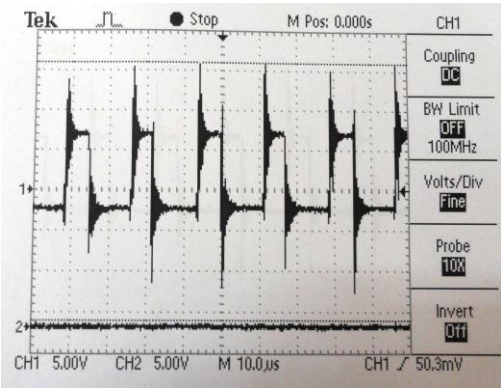

V		T	G	I	S	V	Weld bead
		8	13	166	37	23.7	
		H		W		P	
		3.78		7.81		1.82	

Table 3.29

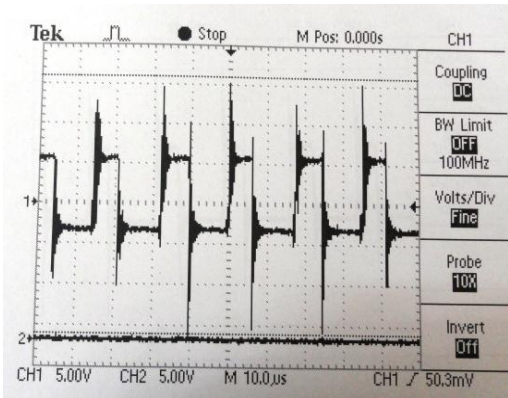

V		T	G	I	S	V	Weld bead
		8	13	241	37		
		H		W		P	
		3.47		7.71		1.89	

Table 3.30

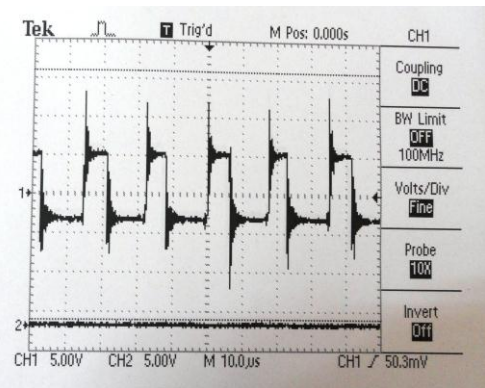

V		T	G	I	S	V	Weld bead
		8	13	241	37	23.7	
		H		W		P	
		3.44		7.79		1.91	

Table 3.31

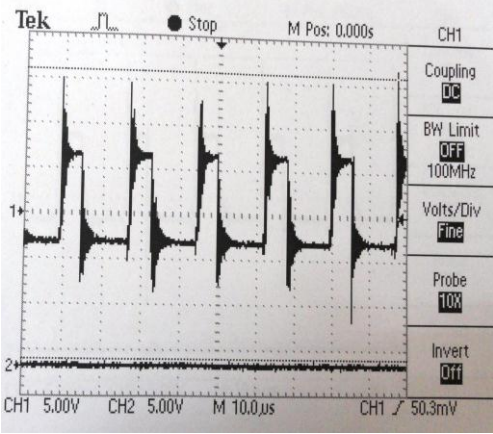
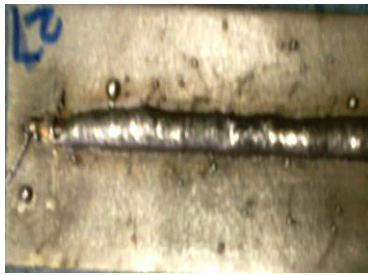
V		T	G	I	S	V	Weld bead
		8	13	241	37	23.7	
		H		W		P	
		3.47		7.78		1.9	

Table 3.32

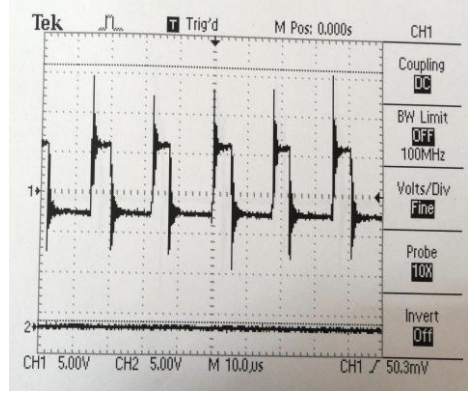

V		T	G	I	S	V	Weld bead
		8	13	241	37	23.4	
		H		W		P	
		3.46		7.52		1.93	

Table 3.33

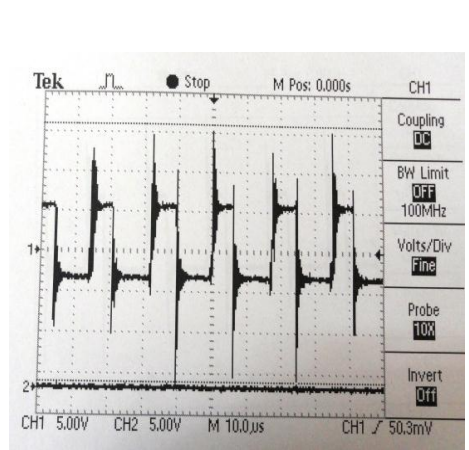

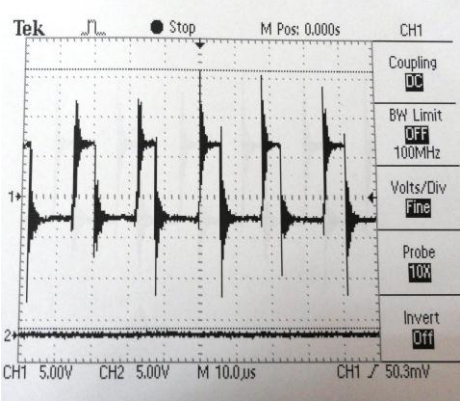

V		T	G	I	S	V	Weld bead
		8	13	241	37	23.4	
		H		W		P	
		3.52		7.73		1.92	

Table 3.34

V		T	G	I	S	V	Weld bead
		8	13	241	37	24.3	
		H		W		P	
		3.45		7.78		1.89	